

Analysis-aware defeaturing of complex geometries with Neumann features

P. Antolín¹ and O. Chanon²

pablo.antolin@epfl.ch, online.chanon@asc.tuwien.ac.at

¹ Institute of Mathematics, École Polytechnique Fédérale de Lausanne, Switzerland

² Institute of Analysis and Scientific Computing, TU Wien, Austria

August 17, 2023

Abstract

Local modifications of a computational domain are often performed in order to simplify the meshing process and to reduce computational costs and memory requirements. However, removing geometrical features of a domain often introduces a non-negligible error in the solution of a differential problem in which it is defined. In this work, we extend the results from [1] by studying the case of domains containing an arbitrary number of distinct Neumann features, and by performing an analysis on Poisson's, linear elasticity, and Stokes' equations. We introduce a simple, computationally cheap, reliable, and efficient *a posteriori* estimator of the geometrical defeaturing error. Moreover, we also introduce a geometric refinement strategy that accounts for the defeaturing error: Starting from a fully defeatured geometry, the algorithm determines at each iteration step which features need to be added to the geometrical model to reduce the defeaturing error. These important features are then added to the (partially) defeatured geometrical model at the next iteration, until the solution attains a prescribed accuracy. A wide range of two- and three-dimensional numerical experiments are finally reported to illustrate this work.

Keywords: Geometric defeaturing, geometric refinement, *a posteriori* error estimation, adaptivity, mesh generation.

AMS Subject Classification: 65N50, 65N30.

1 Introduction

With the advance of engineering knowledge, simulations are performed on objects of increasing geometric complexity, nowadays mainly described by three-dimensional Computer-Aided Design (CAD) models. These models often contain a large number of geometric details of different scales, also called geometric features. Unfortunately, the construction of a finite element mesh on such complex domains may fail, or if it does not, the mesh generation may be very difficult; see for example [2] dealing with the complexity arising from an automatic all-hexahedral mesh generation for complex B-Reps (boundary representations). Moreover, the resulting mesh may require a very large number of elements, therefore leading to simulations which are too costly or even unfeasible. For instance, it has been shown in [3, 4] that the cost of the underlying simulation may be increased by up to a factor 10 in the presence of a single geometric feature of relatively small size.

However, depending on the problem at hand, such high model complexity may be unnecessary. That is, the geometric description of the object may require a high number of degrees of freedom, but not all of them are needed to perform an accurate analysis, and taking all of them into account is potentially too costly. To deal with complex geometries and to accelerate the process of analysis-aware geometric design, it is therefore essential to be able to simplify the geometric model, process also known as defeaturing. This is a very common practice among finite element analysts. See, as matter of example, the case illustrated in Figure 1. There, a CAD design with numerous features as holes, rounds, and a carved logo (Figure 1a) is defeatured to create a simpler model (Figure 1b) that is easier to mesh. Each finite element mesh in Figure 1 was generated using Gmsh [5] with the same mesh algorithm and parameters. Nevertheless, the mesh of the original design has 5 times more nodes than the one of the defeatured model. Likely, most of those extra

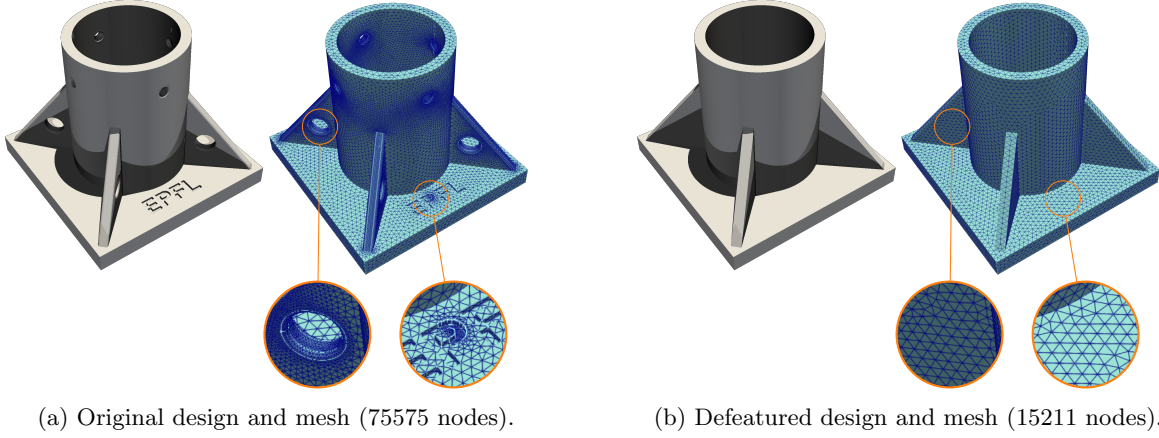


Figure 1: Example of an original (left) and defeatured CAD designs (right). Both finite element meshes were generated with Gmsh [5] using the same mesh algorithm and parameters.

degrees of freedom, required for correctly representing the geometrical details, will improve little the accuracy of the solution obtained with such mesh, but will increase the computational cost and memory requirements significantly.

Nevertheless, it is important to consider how such geometrical simplifications will impact the analysis solution, i.e., to control the error introduced by defeaturing, in order to provide an accurate solution of the problem at hand. The literature on the subject is still relatively scarce, and a lot remains to be done. To estimate the defeaturing error on the solution of a partial differential equation (PDE), some *a posteriori* criteria have been developed: The one introduced in [6] uses an approximation of the error in energy norm; in [7, 8], an estimator is found using topological sensitivity analysis; adjoint theory is used in the series of works [9–11] to describe the first order defeaturing error on a quantity of interest; an estimator is introduced in [12] based on the reciprocal theorem stating the conservation of solution flux in the features; and in the series of works [13–16], defeaturing error is expressed as a modeling error directly on the differential problem, both for negative features (holes) and positive ones (protrusions). In these latter papers, the modeling error is then estimated with the dual weighted residual method [17]. Nevertheless, very few of those works come with a sound mathematical theory, and most of them rely on some heuristics.

In the recent paper [1], the authors have tackled this issue: A precise mathematical framework is defined for geometries for which a single feature of very generic shape is removed, and an efficient and reliable *a posteriori* estimator of the defeaturing error is derived in the context of Poisson’s equation in the energy norm. Worth mentioning related research papers include [18–20] that study heterogeneous and perforated materials, [21] that are interested in the error introduced by the approximation of boundary conditions, and [22] that more generally studies modeling errors coming from dimension reduction, homogenization and model simplification.

We generalize here the work [1]. The original contributions of the presented research are the following:

- We consider geometries for which an *arbitrary number* N of distinct Neumann geometrical features are removed from the computational domain, and we introduce a defeaturing error estimator whose effectivity index is independent from N . Note in particular that the features do not need to be small.
- We do not only consider Poisson’s equation, but also *linear elasticity and Stokes’ problems*. While the considered problems are exclusively linear, the proposed estimator could be extended to encompass nonlinear problems as well.
- Based on the proposed defeaturing error estimator, an *adaptive strategy for geometric refinement* is

introduced: The algorithm begins with a completely simplified geometry and, at each iteration, identifies the necessary features to be added to the geometric model in order to reduce the defeaturing error.

- Finally, more complex *numerical experiments* with engineering interest are presented, in particular the simulation of a three-dimensional CAD design.

The error estimator formulation depends on the problem at hand. Hence, in this work, different expressions will be provided for the Poisson, Stokes, and linear elasticity problems. In particular, the differential problems and their corresponding defeaturing error estimator depend on the material properties and on the boundary conditions. E.g., some features will play more or less predominant roles depending on the chosen boundary conditions.

In general, and in practice, differential problems cannot be solved exactly, and thus a numerical method is used to solve them approximately in a finite dimensional space. However, in this article, we neglect the contribution of the error coming from the numerical approximation of the solution, as we concentrate our efforts on the defeaturing error. Deriving an estimator that also includes the numerical error contribution is the subject of a subsequent work, see [23, 24]. An early method for defeaturing and coarsening, called composite finite elements and developed by Hackbusch and Sauter in [25, 26], deserves mentioning. It assumes that defeaturing arises solely from the limitation of the mesh in resolving geometric details within the computational domain. In contrast, our approach aims to treat defeaturing independently of any discretization, allowing us to separate the strict defeaturing error from the numerical approximation error.

Therefore, in Section 2, we first introduce the problem of defeaturing and the corresponding notation that will be used throughout the article, and we precisely define the defeaturing error that we aim at estimating. Then, we state the main results that are obtained, namely the reliability and the efficiency of an *a posteriori* estimator of the defeaturing error whose effectivity index is independent from the number of the features and their size. Subsequently, in Sections 3 and 4, we precisely define the exact and defeatured problems when the differential problem at hand is, respectively, Poisson's and the linear elasticity or Stokes' equations, and we propose in each case a defeaturing error estimator. We then introduce in Section 5 an adaptive geometric refinement strategy driven by the defeaturing error estimators previously defined. We perform in Section 6 a validation of the presented theory, of the aforementioned estimators' properties, and of the proposed adaptive strategy, thanks to an extensive set of two- and three-dimensional numerical experiments. To perform these tests, we use isogeometric analysis (IGA) [27, 28] on very fine meshes, in order to have a negligible numerical error with respect to the defeaturing error. Since IGA and defeaturing both pursue the scope of reducing the gap between the design and the analysis phases, IGA is a natural method of choice. Nevertheless, it is important to remark that the proposed techniques are completely discretization agnostic and any other numerical method could be used. Some conclusions are finally drawn in Section 7. In the Appendix A, the reliability and efficiency of the proposed defeaturing error estimator are demonstrated in the framework of Stokes' equations, as the proofs for Poisson's and the linear elasticity equations are very similar, easier, and can be found in details in the corresponding thesis [24].

In the following, the operator \lesssim is used to mean any inequality which neither depends on the number of features nor on their size, but which can depend on their shape, on their type (i.e., whether they are holes, also called negative features, or protrusions, also called positive features), and on the space dimension $n = 2$ or $n = 3$. Moreover, for all $D \subset \mathbb{R}^n$, and for all $\Lambda \subset \partial D$, we denote by $|D|$ the n -dimensional Lebesgue measure of D , by $|\Lambda|$ the $(n - 1)$ -dimensional Hausdorff measure of Λ , by \overline{D} and $\overline{\Gamma}$ the closure of D and of Γ , respectively, and by $\text{int}(D)$ and $\text{int}(\Lambda)$ the interior of D and of Γ , respectively.

2 Analysis-aware defeaturing

2.1 Presentation of the problem

In this section, we present the considered problem, following and extending the setting in [1]. Let us consider a potentially complicated, connected open Lipschitz domain $\Omega \subset \mathbb{R}^n$, $n = 2$ or $n = 3$, on which we want to solve a differential problem $\mathcal{P}(\Omega)$ which contains some boundary conditions. More precisely, let us assume that Ω

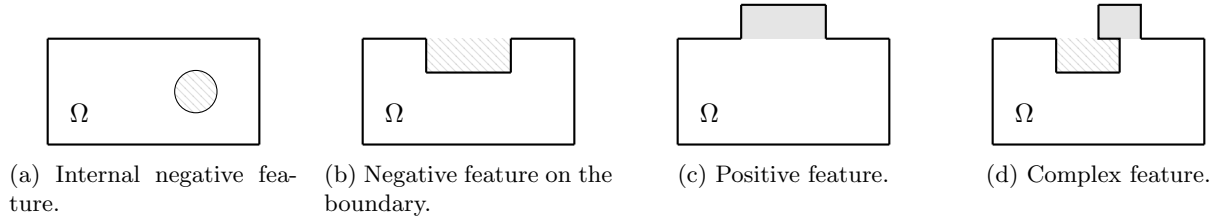


Figure 2: Domains with different types of geometrical features F . In each case, the negative component of F is dashed while its positive component is filled in gray.

contains geometrical details of smaller scale also called features, and assume that the feature information of Ω is known *a priori*. As illustrated in Figure 2, we say that a feature $F \subset \mathbb{R}^n$ is *negative* if $(\overline{F} \cap \Omega) \subset \partial\Omega$, *positive* if $F \subset \Omega$, or *complex* if it has both negative and positive components. A negative feature corresponds to a part where some material has been removed (e.g., a hole), a positive feature corresponds to the addition of some material (e.g., a protrusion), and a feature is complex in the most general situation in which there has been both the addition and the removal of some material. Note that an internal feature (e.g., an internal hole) is a special case of negative feature. We assume that the positive and the negative part of each feature is a connected open Lipschitz domain of \mathbb{R}^n .

However, solving the given differential problem $\mathcal{P}(\Omega)$ can be very complicated due to the complexity of Ω , coming from the presence of the features. Therefore, we solve instead a similar problem but in a *defeatured domain* Ω_0 , where the features of Ω are removed: Holes are filled with some material and protrusions are cut out of the computational domain. This differential problem on Ω_0 is denoted by $\mathcal{P}(\Omega_0)$ and it is called *defeatured* (or simplified) *problem*.

The defeaturing of the computational domain introduces an error in the problem's solution, and we are interested in controlling the energy norm of this so-called *defeating error*. In other words, if u is the solution of the exact problem $\mathcal{P}(\Omega)$ and u_0 is the solution of the defeatured problem $\mathcal{P}(\Omega_0)$, then we are interested in controlling the error “ $u - u_0$ ” in the exact energy norm, which is the energy norm defined by problem $\mathcal{P}(\Omega)$ and denoted as $||| \cdot |||_{\Omega}$. Since u is defined in Ω and u_0 is defined in Ω_0 , the defeating error needs to be more accurately defined. To do so, we need to introduce some further geometric notation.

Generalizing the work from [1], let $N_f \geq 1$, $N_f \in \mathbb{N}$, denote the total number of (possibly complex) features of Ω , gathered into the set $\mathfrak{F} := \{F^k\}_{k=1}^{N_f}$. Let us make the following assumption on the features.

Assumption 2.1 The features in \mathfrak{F} are separated, that is,

- (a) $\overline{F^k} \cap \overline{F^\ell} = \emptyset$ for every $k, \ell = 1, \dots, N_f$, $k \neq \ell$,
- (b) one cannot have an increasingly large number of features that are arbitrarily close to one another.

Remark 2.2 In the currently considered setting, features are discrete objects. Note that:

- It is always possible to satisfy condition (a) of Assumption 2.1 by changing the numbering of the features. Indeed, if there are $k, \ell = 1, \dots, N_f$, $k \neq \ell$, such that $\overline{F^k} \cap \overline{F^\ell} \neq \emptyset$, then $F^{k,\ell} := \text{int}(\overline{F^k} \cup \overline{F^\ell})$ can be considered as a single feature that replaces the two features F^k and F^ℓ . However, note that the treatment of a geometry in which the boundary is complicated everywhere (for instance a fractal-like domain) is not considered here, see instead [29–31] for first results in this different framework.
- The precise mathematical definition of condition (b) will be given at the end of Section 2.3, as it requires technical geometric definitions that would hinder here the readability of the main results of this manuscript.

Since the features in \mathfrak{F} are assumed to be generally complex, this means that, for all $k = 1, \dots, N_f$, the feature $F^k \in \mathfrak{F}$ is an open domain which is composed of a (not necessarily connected) negative component F_n^k ,

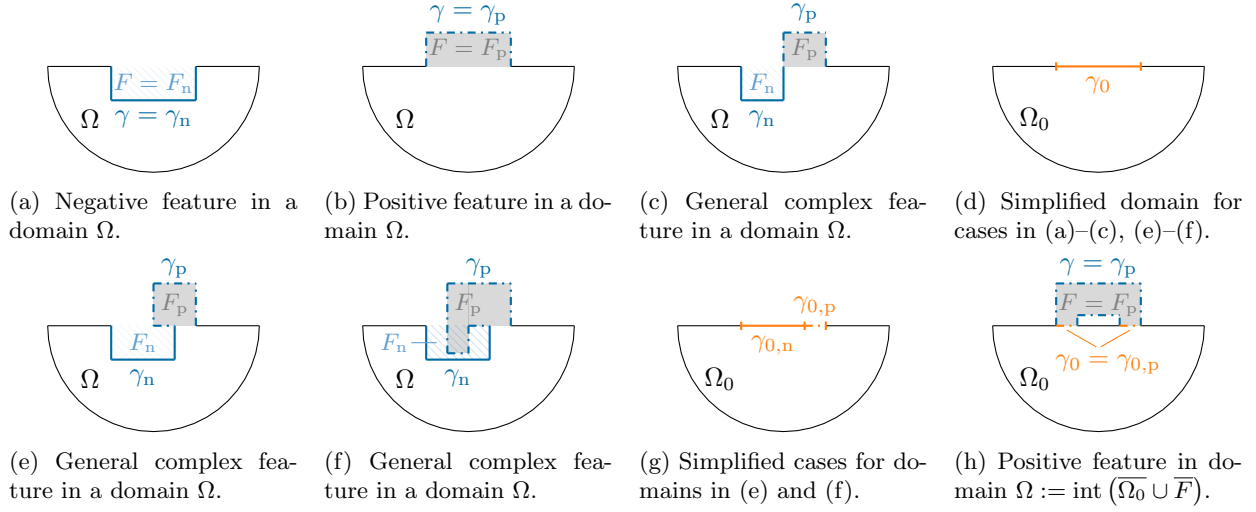


Figure 3: Geometries containing different types of features.

a hole, and a (not necessarily connected) positive component F_p^k , a protrusion, that can have a non-empty intersection, see Figure 3. More precisely,

$$F^k = \text{int} \left(\overline{F_p^k} \cup \overline{F_n^k} \right),$$

where F_n^k and F_p^k are open domains such that, if we define

$$F_p := \text{int} \left(\bigcup_{k=1}^{N_f} \overline{F_p^k} \right), \quad F_n := \text{int} \left(\bigcup_{k=1}^{N_f} \overline{F_n^k} \right), \quad \Omega_\star := \Omega \setminus \overline{F_p}, \quad (1)$$

then

$$F_p \subset \Omega \text{ and } (\overline{F_n} \cap \overline{\Omega_\star}) \subset \partial\Omega_\star.$$

In this setting, we define the defeatured geometry by

$$\Omega_0 := \text{int}(\overline{\Omega_\star} \cup \overline{F_n}) \subset \mathbb{R}^n. \quad (2)$$

Note that in the case in which the exact domain Ω contains a single feature F , i.e. $N_f = 1$, then

- if F is negative, i.e., $F_p = \emptyset$ and $F_n = F$, then $\Omega_0 := \text{int}(\overline{\Omega} \cup \overline{F})$,
- if F is positive, i.e., $F_p = F$ and $F_n = \emptyset$, then $\Omega_0 := \Omega \setminus \overline{F}$,
- if F is complex, definitions (1) and (2) and apply,

therefore generalizing the definition of Ω_0 given in [1].

Remark 2.3 Given a complicated geometry Ω without any further information, one cannot always easily tell whether the features it contains are negative or positive, see Figure 4. Therefore, this is often a choice that the user needs to make, based on the available geometric information at hand. If one has access to a simplified geometry, for instance thanks to the history of CAD operations from which the exact geometry Ω is built, then it is possible to define the features from Ω and Ω_0 , instead of defining Ω_0 from Ω and the features. The identification of features in a given geometry and the construction of a corresponding simplified geometric model can be complicated tasks, see [32] for a review of possible techniques. However, this goes beyond the scope of this work, which supposes at its roots that the feature information is known *a priori*.

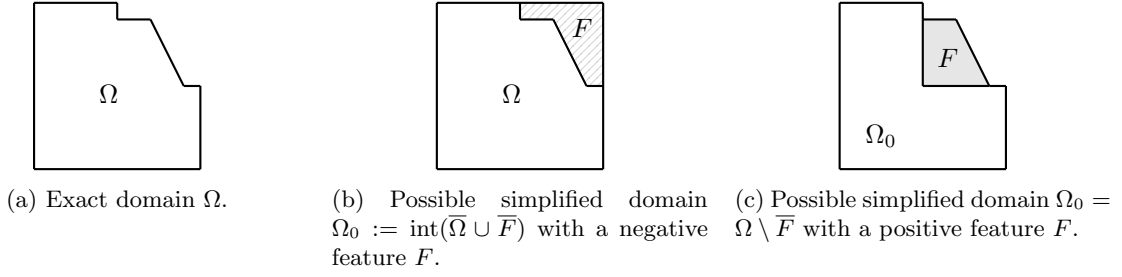


Figure 4: Exact geometry Ω and different possible defeatured geometries Ω_0 .

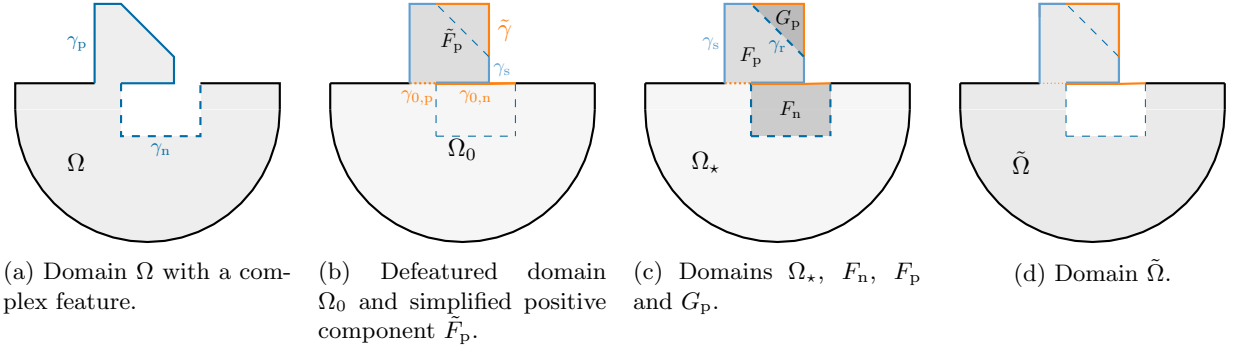


Figure 5: Domain with one complex feature and illustration of the notation. The different domains are distinguished by different gray intensities.

Now, we remark that the solution u_0 of $\mathcal{P}(\Omega_0)$ is not defined in F_p , i.e., in the positive component of the features of Ω , since $F_p \not\subset \Omega_0$ but $F_p \subset \Omega$. Thus, to be able to compare u and u_0 in F_p , we need to solve for each feature $F^k \in \mathfrak{F}$ a local differential problem $\mathcal{P}(F_p^k)$ in F_p^k , whose solution suitably extends u_0 to F_p^k . However, and as already noted in [1], the domain F_p^k might be complicated or even non-smooth, thus finding the solution of the extension problem $\mathcal{P}(F_p^k)$ might be cumbersome. To circumvent this difficulty, instead of solving $\mathcal{P}(F_p^k)$, we solve an extension problem $\mathcal{P}(\tilde{F}_p^k)$ in a simpler domain \tilde{F}_p^k containing F_p^k , see Figure 5. Let us call u_k the solution of $\mathcal{P}(\tilde{F}_p^k)$. The domain \tilde{F}_p^k can be for instance the bounding box of F_p^k , if the solution u_k restricted to F_p^k correctly defines an extension of u_0 in F_p^k , see Section 2.3, Equation (4). Then we define the *extended defeatured solution* u_d in Ω as

$$u_d \equiv \begin{cases} u_0|_{\Omega_\star} & \text{in } \Omega_\star \\ u_k|_{F_p^k} & \text{in } F_p^k, \text{ for all } k = 1, \dots, N_f, \end{cases} \quad (3)$$

where we recall the definition of Ω_\star from (1). We are now finally able to precisely define the defeaturing error in the energy norm by $\|u - u_d\|_\Omega$.

2.2 Main results

In this article, we will precisely define the considered differential problems $\mathcal{P}(\Omega)$, $\mathcal{P}(\Omega_0)$, and $\mathcal{P}(\tilde{F}_p^k)$ for all $k = 1, \dots, N_f$ in the context of Poisson's, linear elasticity, and Stokes' equations. Note that when the linear elasticity equations are considered, then u , u_0 , u_k , and u_d are vector-valued functions that we will also, respectively, write \mathbf{u} , \mathbf{u}_0 , \mathbf{u}_k , and \mathbf{u}_d . Similarly, for Stokes equations, u , u_0 , u_k , and u_d also include the pressure, i.e., we will write them (\mathbf{u}, p) , (\mathbf{u}_0, p_0) , (\mathbf{u}_k, p_k) , and (\mathbf{u}_d, p_d) , respectively.

For each case, we will then define an *a posteriori* estimator $\mathcal{E}(u_d)$ of the defeaturing error in the energy

norm (Sections 3 and 4), in the case in which Neumann boundary conditions are imposed on the boundaries of the features. This assumption is formalized as follows:

Assumption 2.4 Let us decompose $\partial\Omega = \overline{\Gamma_D} \cup \overline{\Gamma_N}$ such that Dirichlet boundary conditions are imposed on Γ_D with $|\Gamma_D| > 0$, Neumann boundary conditions are imposed on Γ_N , and $\Gamma_D \cap \Gamma_N = \emptyset$. Then we assume that for all $k = 1, \dots, N_f$,

$$\Gamma_D \cap (\partial F_n^k \cup \partial F_p^k) = \emptyset.$$

Then for each one of the differential problems $\mathcal{P}(\Omega)$ that will be considered in this article, the introduced *a posteriori* defeaturing error estimator $\mathcal{E}(u_d)$ verifies the two following Theorems 2.5 and 2.7.

Theorem 2.5 (Reliability) *Under Assumptions 2.1 and 2.4, the defeaturing error estimator $\mathcal{E}(u_d)$ is reliable, meaning that it is an upper bound for the defeaturing error in the energy norm:*

$$\|u - u_d\|_\Omega \lesssim \mathcal{E}(u_d).$$

Before stating Theorem 2.7, let us just introduce the following definition.

Definition 2.6 Let Λ be an $(n-1)$ -dimensional subset of \mathbb{R}^n . We say that Λ is *regular* if Λ is piecewise smooth and shape regular, that is, if there exists $N_\Lambda \in \mathbb{N} \setminus \{0\}$ such that for all $\ell_1, \ell_2 = 1, \dots, N_\Lambda$ with $\ell_1 \neq \ell_2$, $\Lambda = \text{int} \left(\bigcup_{\ell=1}^{N_\Lambda} \overline{\Lambda^\ell} \right)$, $\Lambda^{\ell_1} \cap \Lambda^{\ell_2} = \emptyset$, $|\Lambda| \lesssim |\Lambda^{\ell_1}|$ where the hidden constant may depend on N_Λ but not on the measure of each component Λ^{ℓ_1} , and Λ^{ℓ_1} is smooth.

Theorem 2.7 (Efficiency) *Under Assumptions 2.1 and 2.4, if the boundaries of the features are shape regular as in Definition 2.6, then the defeaturing error estimator $\mathcal{E}(u_d)$ is efficient up to oscillations, meaning that it is a lower bound for the defeaturing error in the energy norm:*

$$\mathcal{E}(u_d) \lesssim \|u - u_d\|_\Omega + \text{osc}(u_d),$$

where $\text{osc}(u_d)$ is a higher order term with respect to the size of the features.

We remark again that the inequalities in Theorems 2.5 and 2.7 do not depend neither on the size nor on the number of features. In addition, as it will be shown in Sections 3 and 4 for Poisson, Stokes, and linear elasticity problems, the estimator $\mathcal{E}(u_d)$ is simple and computationally cheap, and it is not only driven by geometrical considerations, but also by the PDE at hand.

The explicit expression of the oscillation term $\text{osc}(u_d)$ will be provided in Appendix A, together with the proofs of Theorems 2.5 and 2.7, in the framework of Stokes' equations, as the oscillations corresponding to Poisson's and linear elasticity equations are very similar and their details can be found in [24]. The key issue in the analysis is to track the dependence of all constants from the sizes of the features and from their number.

2.3 Some further geometric notation

To be able to correctly define the defeaturing error estimator $\mathcal{E}(u_d)$, we need to introduce some further notation identifying specific pieces of boundaries of the features. In the following, we use the upper index k to refer to the feature F^k , with $k = 1, \dots, N_f$, and the lower indices n and p to refer to negative and positive components of the features, respectively.

Now in particular, we let γ be the union of the pieces of boundaries of Ω that are removed by defeaturing, and we let γ_0 be the union of the pieces of boundaries of Ω_0 replacing them, that is, and as illustrated in

Figure 3,

$$\gamma_0 := \bigcup_{k=1}^{N_f} \gamma_0^k \quad \text{and} \quad \gamma := \bigcup_{k=1}^{N_f} \gamma^k,$$

where $\gamma_0^k := \text{int}(\overline{\gamma_{0,n}^k} \cup \overline{\gamma_{0,p}^k}) \subset \partial\Omega_0$ with $\gamma_{0,n}^k := \partial F_n^k \setminus \partial\Omega_\star$, $\gamma_{0,p}^k := \partial F_p^k \setminus \partial\Omega$,

$$\gamma^k := \text{int}(\overline{\gamma_n^k} \cup \overline{\gamma_p^k}) \subset \partial\Omega \quad \text{with} \quad \gamma_n^k := \partial F_n^k \setminus \overline{\gamma_{0,n}^k}, \quad \gamma_p^k := \partial F_p^k \setminus \overline{\gamma_{0,p}^k},$$

so that $\partial F_n^k = \overline{\gamma_n^k} \cup \overline{\gamma_{0,n}^k}$ with $\gamma_n^k \cap \gamma_{0,n}^k = \emptyset$, and $\partial F_p^k = \overline{\gamma_p^k} \cup \overline{\gamma_{0,p}^k}$ with $\gamma_p^k \cap \gamma_{0,p}^k = \emptyset$. Moreover, let

$$\gamma_{0,n} := \bigcup_{k=1}^{N_f} \gamma_{0,n}^k, \quad \gamma_{0,p} := \bigcup_{k=1}^{N_f} \gamma_{0,p}^k,$$

$$\gamma_n := \bigcup_{k=1}^{N_f} \gamma_n^k, \quad \gamma_p := \bigcup_{k=1}^{N_f} \gamma_p^k.$$

Using this notation and following the discussion in Section 2.1, we can now precisely determine which simple extension \tilde{F}_p^k of the positive component F_p^k can be chosen, for all $k = 1, \dots, N_f$ (see Figure 5). More precisely, for the solution of $\mathcal{P}(\tilde{F}_p^k)$ restricted to F_p^k to correctly define an extension of the solution of $\mathcal{P}(\Omega_0)$ in F_p^k , we need

$$\tilde{F}_p^k \supset F_p^k, \quad \gamma_{0,p}^k \subset (\partial \tilde{F}_p^k \cap \partial F_p^k). \quad (4)$$

Note that it is possible to have $\tilde{F}_p^k \cap \Omega_0 \neq \emptyset$. Let us also define

$$G_p^k := \tilde{F}_p^k \setminus \overline{F_p^k} \quad \text{for all } k = 1, \dots, N_f \quad \text{and} \quad G_p := \bigcup_{k=1}^{N_f} G_p^k.$$

We remark that for all $k = 1, \dots, N_f$, one can look at \tilde{F}_p^k as the defeatured geometry of the positive component F_p^k , that is, as a geometry simplified from the exact geometry F_p^k , for which G_p^k is a negative feature (see Figure 5c). To simplify the following exposition, and even if this hypothesis could easily be removed, let us make the following assumption regarding these domain extensions.

Assumption 2.8 Let us assume that

- $\tilde{F}_p^k \cap \tilde{F}_p^\ell = \emptyset$ for all $k, \ell = 1, \dots, N_f$ such that $k \neq \ell$,
- if we let $\tilde{F}_p := \bigcup_{k=1}^{N_f} \tilde{F}_p^k$, then $\tilde{F}_p \cap \Omega_\star = \emptyset$ for all $k = 1, \dots, N_f$.

In addition, let $\tilde{\gamma}^k := \partial \tilde{F}_p^k \setminus \partial F_p^k$, and let γ_p^k be decomposed as $\gamma_p^k = \text{int}(\overline{\gamma_s^k} \cup \overline{\gamma_r^k})$, being γ_s^k and γ_r^k open, γ_s^k is the part of γ_p^k , that is shared with $\partial \tilde{F}_p^k$, while γ_r^k is the remaining part of γ_p^k , that is, the part that does not belong to $\partial \tilde{F}_p^k$. I.e., $\gamma_s^k = \gamma_p^k \cap \partial \tilde{F}_p^k$ and $\gamma_r^k = \gamma_p^k \setminus \gamma_s^k$. This notation is illustrated in Figure 5. Then, similarly to the previously introduced notation, let

$$\tilde{\gamma} := \bigcup_{k=1}^{N_f} \tilde{\gamma}^k, \quad \gamma_s := \bigcup_{k=1}^{N_f} \gamma_s^k, \quad \gamma_r := \bigcup_{k=1}^{N_f} \gamma_r^k.$$

In the sequel, we will see that the boundaries γ_n , $\gamma_{0,p}$, and γ_r will play an important role in the definition of the defeaturing error estimators $\mathcal{E}(u_d)$. Therefore, let us also introduce the following notation:

$$\Gamma^k := \gamma_n^k \cup \gamma_{0,p}^k \cup \gamma_r^k, \quad \text{for } k = 1, \dots, N_f, \quad (5)$$

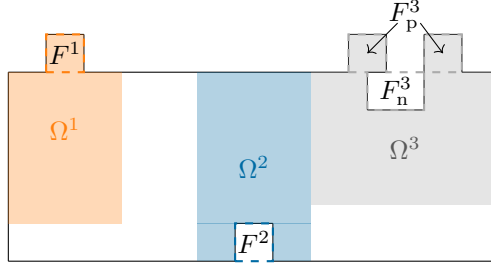


Figure 6: Domain Ω with three separated features, and a possible choice of subdomains Ω^k , $k = 1, 2, 3$, satisfying Assumption 2.1.

and the sets

$$\begin{aligned}\Sigma_n &:= \{\gamma_n^k\}_{k=1}^{N_f}, \quad \Sigma_{0,p} := \{\gamma_{0,p}^k\}_{k=1}^{N_f}, \quad \Sigma_r := \{\gamma_r^k\}_{k=1}^{N_f}, \\ \Sigma^k &:= \{\gamma_n^k, \gamma_{0,p}^k, \gamma_r^k\}, \quad \text{for } k = 1, \dots, N_f, \\ \Sigma &:= \{\gamma \in \Sigma^k : k = 1, \dots, N_f\}.\end{aligned}\tag{6}$$

Finally, let \mathbf{n} and \mathbf{n}_0 respectively denote the unit outward normal vectors to Ω and Ω_0 . Moreover, for all $k = 1, \dots, N_f$, let $\tilde{\mathbf{n}}^k$ be the unitary outward normal to \tilde{F}_p^k , and let $\mathbf{n}^k \equiv \mathbf{n}_{F^k}$ denote the unitary outward normal vector to F_n^k and to F_p^k . Note that the vectors \mathbf{n}^k may not be uniquely defined if the outward normal to F_n^k is of opposite sign of the outward normal to F_p^k (see Figure 5 for instance), but we allow this abuse of notation since the context will always make it clear.

With this technical notation at hand, we can now precisely restate condition (b) of Assumption 2.1.

Assumption 2.1 (b) There exist sub-domains $\Omega^k \subset \Omega$, $k = 1, \dots, N_f$ such that

- $F_p^k \subset \Omega^k$, $(\gamma_n^k \cup \gamma_r^k) \subset \partial\Omega^k$, $\gamma_{0,p}^k \subset \partial(\Omega^k \cap \Omega_0)$,
- $|\Omega^k| \simeq |\Omega|$ where the hidden constant is independent of the size of the features, i.e., the measure of Ω^k is comparable with the measure of Ω , not with the measure of the feature F^k ,
- $N_s := \max_{J \subset \{1, \dots, N_f\}} \left(\#J : \bigcap_{k \in J} \Omega^k \neq \emptyset \right) \ll N_f$, that is, the maximum number N_s of superposed sub-domains Ω^k is limited and notably smaller than the total number of features N_f .

This condition is illustrated in Figure 6. Note that if $N_f = 1$, one can take $\Omega^1 := \Omega$.

3 Defeating in Poisson's equation

In this section, we consider the Poisson equation and precisely define the exact problem $\mathcal{P}(\Omega)$, the defeated problem $\mathcal{P}(\Omega_0)$, and the extension problems $\mathcal{P}(\tilde{F}_p^k)$ for all $k = 1, \dots, N_f$. Then in this context, we give a precise definition of the proposed reliable and efficient *a posteriori* estimator $\mathcal{E}(u_d)$ of the energy norm of the defeating error $\|u - u_d\|_\Omega$.

In the following, we denote by $H^s(D)$ the Sobolev space of order $s \in \mathbb{R}$ in a domain $D \subset \mathbb{R}^n$, whose classical norm and semi-norm are written $\|\cdot\|_{s,D}$ and $|\cdot|_{s,D}$, respectively. We will also denote by $L^2(D) := H^0(D)$. Moreover, if we let $\varphi \subset \partial D$ and $z \in H^{\frac{1}{2}}(\varphi)$, and to be able to deal with boundary conditions, we will denote by

$$H_{z,\varphi}^1(D) := \{y \in H^1(D) : \text{tr}_\varphi(y) = z\},$$

where $\text{tr}_\varphi(y)$ denotes the trace of y on φ .

3.1 Exact and defeatured problems

Let us first introduce Poisson's problem $\mathcal{P}(\Omega)$ in the exact geometry Ω . To do so, let $g_D \in H^{\frac{3}{2}}(\Gamma_D)$, $g \in H^{\frac{1}{2}}(\Gamma_N)$ and $f \in L^2(\Omega)$. Note that one order of regularity more than usual is required. As we will further see, to define the proposed defeaturing error estimator, we need a solution whose normal derivative along the features' boundaries belongs to L^2 . Then, the problem reads: find $u \in H_{g_D, \Gamma_D}^1(\Omega)$, the weak solution of

$$\mathcal{P}(\Omega) : \begin{cases} -\Delta u = f & \text{in } \Omega \\ u = g_D & \text{on } \Gamma_D \\ \frac{\partial u}{\partial \mathbf{n}} = g & \text{on } \Gamma_N, \end{cases} \quad \text{i.e., } \forall v \in H_{0, \Gamma_D}^1(\Omega), \quad \mathbf{a}(u, v) := \int_{\Omega} \nabla u \cdot \nabla v \, dx = \int_{\Omega} f v \, dx + \int_{\Gamma_N} g v \, ds. \quad (7)$$

If $H_{0, \Gamma_D}^1(\Omega)$ is equipped with the $L^2(\Omega)$ -norm of the gradient $\|\nabla \cdot\|_{0, \Omega}$, then we know from Riesz representation theorem that this problem is well-posed. However, note that this problem is usually not solved in practice, as it is assumed to be computationally expensive.

Let us therefore introduce the corresponding Poisson problem $\mathcal{P}(\Omega_0)$ in the defeatured geometry Ω_0 . To do so, we need to consider an L^2 -extension of the restriction $f|_{\Omega_*}$ in all the negative components $F_{\mathbf{n}}^k$, $k = 1, \dots, N_f$, that we still write $f \in L^2(\Omega_0)$ by abuse of notation. Note that such an extension is not needed in the positive components of the features. Then instead of (7), we solve the following defeatured Poisson problem: after choosing $g_0 \in H^{\frac{1}{2}}(\gamma_0)$, find $u_0 \in H_{g_D, \Gamma_D}^1(\Omega_0)$, the weak solution of

$$\mathcal{P}(\Omega_0) : \begin{cases} -\Delta u_0 = f & \text{in } \Omega_0 \\ u_0 = g_D & \text{on } \Gamma_D \\ \frac{\partial u_0}{\partial \mathbf{n}_0} = g & \text{on } \Gamma_N \setminus \gamma \\ \frac{\partial u_0}{\partial \mathbf{n}_0} = g_0 & \text{on } \gamma_0, \end{cases} \quad \text{i.e., } \int_{\Omega_0} \nabla u_0 \cdot \nabla v_0 \, dx = \int_{\Omega_0} f v_0 \, dx + \int_{\Gamma_N \setminus \gamma} g v_0 \, ds + \int_{\gamma_0} g_0 v_0 \, ds \quad (8)$$

for all $v_0 \in H_{0, \Gamma_D}^1(\Omega_0)$. Let us recall that, according to Assumption 2.4, $\Gamma_D \cap \gamma = \emptyset$. From the Riesz representation theorem, we know that problem (8) is well-posed.

Remark 3.1 The best possible choices for the defeatured problem data f in $F_{\mathbf{n}}^k$ for $k = 1, \dots, N_f$ and g_0 on γ_0 will be guided by Remark 3.2. However, remark that in applications, the defeatured problem data are rarely chosen, being rather determined by the problem at hand, and being often taken as the natural extension of the exact problem data. For instance, if the right hand side f corresponds to the gravity field, then its only possible physical extension to the negative components of the features is still the gravity field itself. Moreover, one of the aims of defeaturing relies in avoiding the local meshing of the features when the differential problem is solved numerically. Therefore, when the geometry is defeatured, one does not want to have to do a local meshing to capture the behavior of the defeaturing problem data, as this would be equivalent to meshing the feature. We only anticipate here that the best possible defeatured problem data allow the conservation of the solution flux in the positive and negative components of the features. That is, the defeaturing error will be smaller if the defeatured problem data verify for all $k = 1, \dots, N_f$,

$$\int_{\gamma_{0, \mathbf{p}}^k} g_0 \, ds = \int_{\gamma_{\mathbf{p}}^k} g \, ds + \int_{F_{\mathbf{p}}^k} f \, dx, \quad \text{and} \quad \int_{\gamma_{0, \mathbf{n}}^k} g_0 \, ds = \int_{\gamma_{\mathbf{n}}^k} g \, ds - \int_{F_{\mathbf{n}}^k} f \, dx. \quad (9)$$

Now, we need to extend the solution u_0 of (8) to $\tilde{F}_{\mathbf{p}}^k$, for $k = 1, \dots, N_f$, as discussed in Section 2.1, where $\tilde{F}_{\mathbf{p}}^k$ satisfies the properties given in (4). To do so, we need to consider an L^2 -extension of the restriction $f|_{F_{\mathbf{p}}^k}$ in each $G_{\mathbf{p}}^k := \tilde{F}_{\mathbf{p}}^k \setminus \overline{F_{\mathbf{p}}^k}$, that we still write f by abuse of notation. Then, we solve the following extension

problem for $k = 1, \dots, N_f$: after choosing $\tilde{g}^k \in H^{\frac{1}{2}}(\tilde{\gamma}^k)$, find $u_k \in H^1_{u_0, \gamma_{0,p}^k}(\tilde{F}_p^k)$, the weak solution of

$$\mathcal{P}(\tilde{F}_p^k) : \begin{cases} -\Delta u_k = f & \text{in } \tilde{F}_p^k \\ u_k = u_0 & \text{on } \gamma_{0,p}^k \\ \frac{\partial u_k}{\partial \tilde{\mathbf{n}}^k} = \tilde{g}^k & \text{on } \tilde{\gamma}^k \\ \frac{\partial u_k}{\partial \tilde{\mathbf{n}}^k} = g & \text{on } \gamma_s^k, \end{cases} \quad \text{i.e.,} \quad \int_{\tilde{F}_p^k} \nabla u_k \cdot \nabla v^k \, dx = \int_{\tilde{F}_p^k} f v^k \, dx + \int_{\tilde{\gamma}^k} \tilde{g}^k v^k \, ds + \int_{\gamma_s^k} g v^k \, ds \quad (10)$$

for all $v^k \in H^1_{0, \gamma_{0,p}^k}(\tilde{F}_p^k)$. As before, from Riesz representation theorem, we know that problem (10) is well-posed. Once again, the choice of the defeatured problem data f in G_p^k and \tilde{g}^k on $\tilde{\gamma}^k$, for $k = 1, \dots, N_f$, will be guided by Remark 3.2. Thus, as in (8), the best possible choices will allow for the conservation of the solution flux in every feature extension G_p^k . That is, the best possible choices verify for all $k = 1, \dots, N_f$,

$$\int_{\tilde{\gamma}^k} \tilde{g}^k \, ds = \int_{\gamma_r^k} g \, ds - \int_{G_p^k} f \, dx. \quad (11)$$

Then, the defeatured solution $u_d \in H_{g_D, \Gamma_D}(\Omega)$ is defined from u_0 and u_k for $k = 1, \dots, N_f$ as in (3), and the energy norm of the defeaturing error is defined as

$$\|u - u_d\|_{\Omega} := (\mathbf{a}(u - u_d, u - u_d))^{\frac{1}{2}} = \|\nabla(u - u_d)\|_{0, \Omega}. \quad (12)$$

3.2 Defeating error estimator

In this section, we generalize the defeating error estimator introduced in [1], in the case of a geometry that presents multiple features. As for the single feature case, the derived estimator is an upper bound and a lower bound (up to oscillations) of the energy norm of the defeating error.

Let us recall the definition of the defeatured solution u_d from (3), and the definitions of Σ , Σ^k , Σ_n , $\Sigma_{0,p}$, and Σ_r from (6). Then for all $\gamma \in \Sigma$, let $k_{\gamma} \equiv k$ if $\gamma \in \Sigma^k$ for some $k = 1, \dots, N_f$, and let

$$d_{\gamma} \equiv \begin{cases} g - \frac{\partial u_d}{\partial \mathbf{n}} & \text{if } \gamma \in \Sigma_n \text{ or if } \gamma \in \Sigma_r, \\ -\left(g_0 + \frac{\partial u_d}{\partial \mathbf{n}^{k_{\gamma}}}\right) & \text{if } \gamma \in \Sigma_{0,p}. \end{cases} \quad (13)$$

In other words, d_{γ} represents the Neumann error on the boundaries γ_n and γ_r due to the defeating process, and the jump of the normal derivative of the defeatured solution on the boundaries $\gamma_{0,p}$. Then, if we let $\eta \in \mathbb{R}$ be the unique solution of $\eta = -\log(\eta)$, and if for all $\gamma \in \Sigma$, we let

$$c_{\gamma} := \begin{cases} \max(-\log(|\gamma|), \eta)^{\frac{1}{2}} & \text{if } n = 2 \\ 1 & \text{if } n = 3, \end{cases} \quad (14)$$

we define the *a posteriori* defeating error estimator as:

$$\mathcal{E}(u_d) := \left(\sum_{\gamma \in \Sigma} \mathcal{E}_{\gamma}(u_d)^2 \right)^{\frac{1}{2}}, \quad (15)$$

where, for all $\gamma \in \Sigma$,

$$\mathcal{E}_{\gamma}(u_d) := \left(|\gamma|^{\frac{1}{n-1}} \|d_{\gamma} - \overline{d_{\gamma}}^{\gamma}\|_{0, \gamma}^2 + c_{\gamma}^2 |\gamma|^{\frac{n}{n-1}} |\overline{d_{\gamma}}^{\gamma}|^2 \right)^{\frac{1}{2}},$$

where $\overline{d_{\gamma}}^{\gamma}$ denotes the average value of d_{γ} over γ . Note that we can rewrite the estimator feature-wise as follows:

$$\mathcal{E}(u_d) = \left(\sum_{k=1}^{N_f} \sum_{\gamma \in \Sigma^k} \mathcal{E}_{\gamma}(u_d)^2 \right)^{\frac{1}{2}} = \left(\sum_{k=1}^{N_f} \mathcal{E}^k(u_d)^2 \right)^{\frac{1}{2}}, \quad (16)$$

where for all $k = 1, \dots, N_f$, we define $\mathcal{E}^k(u_d)$ as the defeaturing error estimator for feature F^k , that is,

$$\mathcal{E}^k(u_d) := \left(\sum_{\gamma \in \Sigma^k} \mathcal{E}_{\gamma}(u_d)^2 \right)^{\frac{1}{2}}.$$

The proposed estimator indicates that the whole information on the error introduced by defeaturing multiple features, in the energy norm, is encoded in the boundary of the features, and can be accounted by suitably evaluating the error made on the normal derivative of the solution. This result generalizes the one from [1].

Remark 3.2 As analogously noted in [1, Remarks 4.1 and 5.3], the terms involving the average values of d_{γ} in the estimator $\mathcal{E}(u_d)$ only depend on the defeatured problem data since for all $k = 1, \dots, N_f$,

$$\begin{aligned} \overline{d_{\gamma_n^k}}^{\gamma_n^k} &= \overline{\left(g - \frac{\partial u_d}{\partial \mathbf{n}} \right)}^{\gamma_n^k} = \frac{1}{|\gamma_n^k|} \left(\int_{\gamma_n^k} g \, ds - \int_{\gamma_{0,n}^k} g_0 \, ds - \int_{F_n} f \, dx \right), \\ \overline{d_{\gamma_{0,p}^k}}^{\gamma_{0,p}^k} &= \overline{\left(g_0 + \frac{\partial u_d}{\partial \mathbf{n}^k} \right)}^{\gamma_{0,p}^k} = \frac{1}{|\gamma_{0,p}^k|} \left(\int_{\gamma_{0,p}^k} g_0 \, ds - \int_{\gamma_p^k} g \, ds - \int_{F_p^k} f \, dx \right), \\ \overline{d_{\gamma_r^k}}^{\gamma_r^k} &= \overline{\left(g - \frac{\partial u_d}{\partial \mathbf{n}} \right)}^{\gamma_r^k} = \frac{1}{|\gamma_r^k|} \left(\int_{\gamma_r^k} g \, ds - \int_{\tilde{\gamma}^k} \tilde{g}^k \, ds - \int_{\tilde{F}_p^k \setminus F_p^k} f \, dx \right). \end{aligned}$$

As a consequence, if these terms dominate, this means that the defeatured problem data should be more accurately chosen, namely g_0 , \tilde{g}^k , and the extension of f to G_p^k . Moreover, under the reasonable flux conservation assumptions (9) and (11), the defeaturing error estimator (15) rewrites

$$\mathcal{E}(u_d) := \left(\sum_{\gamma \in \Sigma} |\gamma|^{\frac{1}{n-1}} \|d_{\gamma}\|_{0,\gamma}^2 \right)^{\frac{1}{2}}.$$

Remark 3.3 Note that

$$\mathcal{E}(u_d) \lesssim \left(\sum_{\gamma \in \Sigma} c_{\gamma}^2 |\gamma|^{\frac{1}{n-1}} \|d_{\gamma}\|_{0,\gamma}^2 \right)^{\frac{1}{2}} =: \tilde{\mathcal{E}}(u_d).$$

However, when $n = 2$, and under the flux conservation conditions (9) and (11), $\tilde{\mathcal{E}}(u_d)$ is sub-optimal since in this case, $\tilde{\mathcal{E}}(u_d) \lesssim \max_{\gamma \in \Sigma} (c_{\gamma}) \mathcal{E}(u_d)$. Indeed, no lower bound can be provided for $\tilde{\mathcal{E}}(u_d)$.

4 Defeating in linear elasticity and in Stokes' equations

In this section, we consider the linear elasticity and the Stokes equations, and, following the same structure as for the Poisson's problem in Section 3, we define precisely the exact $\mathcal{P}(\Omega)$, defeatured $\mathcal{P}(\Omega_0)$, and extension problems $\mathcal{P}(\tilde{F}_p^k)$ for all $k = 1, \dots, N_f$. Then in this context, we give a precise definition of the proposed a

a posteriori estimator of the energy norm of the defeaturing error, together with the proof of its reliability and efficiency (up to oscillations).

In the following, we denote by $\mathbf{H}^s(D) := [H^s(D)]^n$ the vector-valued Sobolev space of order $s \in \mathbb{R}$ in a domain $D \subset \mathbb{R}^n$, whose classical norm and semi-norm are again written $\|\cdot\|_{s,D}$ and $|\cdot|_{s,D}$, respectively. We will also denote by $\mathbf{L}^2(D) := \mathbf{H}^0(D)$. Moreover, if we let $\varphi \subset \partial D$ and $\mathbf{z} \in \mathbf{H}^{\frac{1}{2}}(\varphi)$, and to be able to deal with boundary conditions, we will denote by

$$\mathbf{H}_{\mathbf{z},\varphi}^1(D) := \{\mathbf{y} \in \mathbf{H}^1(D) : \text{tr}_\varphi(\mathbf{y}) = \mathbf{z}\},$$

where $\text{tr}_\varphi(\mathbf{y})$ denotes the trace of \mathbf{y} on φ .

4.1 Exact and defeatured problems

Let us first introduce the Stokes problem $\mathcal{P}(\Omega)$ in the exact geometry Ω . To do so, considering a function $\mathbf{v} : \Omega \rightarrow \mathbb{R}^n$, let $\boldsymbol{\varepsilon}(\mathbf{v}) := \frac{1}{2}(\nabla \mathbf{v} + \nabla \mathbf{v}^T)$ be the linearized strain rate tensor in Ω and let

$$\boldsymbol{\sigma}(\mathbf{v}) = 2\mu\boldsymbol{\varepsilon}(\mathbf{v}). \quad (17)$$

be the viscous stress tensor of the considered Newtonian fluid, where the constant $\mu > 0$ is the dynamic viscosity. Note that $\boldsymbol{\sigma}(\mathbf{v})$ is the viscous stress tensor and not the total Cauchy stress tensor that would be defined by $\hat{\boldsymbol{\sigma}}(\mathbf{v}, q) := \boldsymbol{\sigma}(\mathbf{v}) - q\mathbb{I}_n$ for some function $q : \Omega \rightarrow \mathbb{R}$ in the space of pressures.

Assumption 4.1 Hereinafter, for the sake of simplicity in the exposition, we assume that λ is constant everywhere, and it is therefore naturally extended to the defeatured geometry Ω_0 .

Now, let $\mathbf{g}_D \in \mathbf{H}^{\frac{3}{2}}(\Gamma_D)$, $\mathbf{g} \in \mathbf{H}^{\frac{1}{2}}(\Gamma_N)$, $f_c \in L^2(\Omega)$, and $\mathbf{f} \in \mathbf{L}^2(\Omega)$. We are interested in the following Stokes problem defined in the exact geometry Ω : find $(\mathbf{u}, p) \in \mathbf{H}_{\mathbf{g}_D, \Gamma_D}^1(\Omega) \times L^2(\Omega)$, the weak solution of

$$\mathcal{P}(\Omega) : \begin{cases} -\nabla \cdot \boldsymbol{\sigma}(\mathbf{u}) + \nabla p = \mathbf{f} & \text{in } \Omega \\ \nabla \cdot \mathbf{u} = f_c & \text{in } \Omega \\ \mathbf{u} = \mathbf{g}_D & \text{on } \Gamma_D \\ \boldsymbol{\sigma}(\mathbf{u})\mathbf{n} - p\mathbf{n} = \mathbf{g} & \text{on } \Gamma_N, \end{cases} \quad \text{i.e.,} \quad \begin{cases} \mathbf{a}(\mathbf{u}, \mathbf{v}) + \mathbf{b}(p, \mathbf{v}) = \int_{\Omega} \mathbf{f} \cdot \mathbf{v} \, dx + \int_{\Gamma_N} \mathbf{g} \cdot \mathbf{v} \, ds \\ \mathbf{b}(q, \mathbf{u}) = - \int_{\Omega} q f_c \, dx \end{cases} \quad (18)$$

for all $(\mathbf{v}, q) \in \mathbf{H}_{0, \Gamma_D}^1(\Omega) \times L^2(\Omega)$, where for all $\mathbf{v}, \mathbf{w} \in \mathbf{H}^1(\Omega)$ and all $q \in L^2(\Omega)$,

$$\mathbf{a}(\mathbf{w}, \mathbf{v}) := \int_{\Omega} \boldsymbol{\sigma}(\mathbf{u}) : \boldsymbol{\varepsilon}(\mathbf{v}) \, dx \quad \text{and} \quad \mathbf{b}(q, \mathbf{v}) := - \int_{\Omega} p \nabla \cdot \mathbf{v} \, dx. \quad (19)$$

If we equip $\mathbf{H}_{0, \Gamma_D}^1(\Omega)$ with the norm $\|\nabla \cdot\|_{0, \Omega}$, it is possible to show by Ladyzhenskaya-Babuška-Brezzi theorem [33] that problem (18) is well-posed. However, note that this problem is never solved in practice, as it is assumed to be computationally too expensive.

Remark 4.2 In a more general setting, the viscous stress tensor writes

$$\boldsymbol{\sigma}(\mathbf{v}) = 2\mu\boldsymbol{\varepsilon}(\mathbf{v}) + \lambda(\nabla \cdot \mathbf{v})\mathbb{I}_n \quad (20)$$

instead of (17), where $\mu > 0$ and $\lambda \geq 0$ are the dynamic and bulk viscosities, respectively, and \mathbb{I}_n is the identity tensor in $\mathbb{R}^{n \times n}$. However, note that in this case,

- if $f_c \equiv 0$, then (18) is the system of equations describing a linear elastic problem in the incompressible limit $\lambda \rightarrow \infty$, and the constitutive relation (20) then simplifies to (17);
- since $\nabla \cdot (\lambda(\nabla \cdot \mathbf{v})\mathbb{I}_n) = \nabla(\lambda \nabla \cdot \mathbf{v})$, if we use the change of variables, $p' := p - \lambda \nabla \cdot \mathbf{u}$ and $\boldsymbol{\sigma}'(\mathbf{u}) := 2\mu\boldsymbol{\varepsilon}(\mathbf{u})$ as in (17), then problem (18) remains identical if we replace p by p' and the general expression $\boldsymbol{\sigma}(\mathbf{u})$ from (20) by $\boldsymbol{\sigma}'(\mathbf{u})$ from (17).

Hence, instead of (20), we choose the simpler expression (17) for σ , without loss of generality.

Remark 4.3 The linear elasticity equations can be obtained from Stokes' equations (18) by removing the pressure terms and the divergence condition. In this case, $\sigma(\mathbf{v})$ is the Cauchy stress tensor in the medium, satisfying Hooke's law, and in the general form (20), λ and μ denote the first and second Lamé coefficients, respectively, with $\mu > 0$ and $\lambda + \frac{2}{3}\mu > 0$. Since the corresponding defeatured problem and the derivation of the defeaturing error estimator for the linear elasticity equations can simply be obtained by removing the pressure terms everywhere, then we will not detail this case and the interested reader is referred to [24].

Now, let us introduce the corresponding Stokes problem $\mathcal{P}(\Omega_0)$ in the defeatured geometry Ω_0 . To do so, we need to choose an L^2 -extension of \mathbf{f} and an L^2 -extension of f_c in the negative components of the features F_n , that we still write \mathbf{f} and f_c by abuse of notation. Moreover, we assume that the viscous stress tensor σ also satisfies (17) on functions defined everywhere in Ω_0 . Then instead of the exact problem (18), the following defeatured problem is solved: after choosing $\mathbf{g}_0 \in \mathbf{H}^{\frac{1}{2}}(\gamma_0)$, find the weak solution $(\mathbf{u}_0, p_0) \in \mathbf{H}^1(\Omega_0) \times L^2(\Omega_0)$ of

$$\mathcal{P}(\Omega_0) : \begin{cases} -\nabla \cdot \sigma(\mathbf{u}_0) + \nabla p_0 = \mathbf{f} & \text{in } \Omega_0 \\ \nabla \cdot \mathbf{u}_0 = f_c & \text{in } \Omega_0 \\ \mathbf{u}_0 = \mathbf{g}_D & \text{on } \Gamma_D \\ \sigma(\mathbf{u}_0)\mathbf{n} - p_0\mathbf{n} = \mathbf{g} & \text{on } \Gamma_N \setminus \gamma \\ \sigma(\mathbf{u}_0)\mathbf{n}_0 - p_0\mathbf{n} = \mathbf{g}_0 & \text{on } \gamma_0, \end{cases} \quad (21)$$

that is, $(\mathbf{u}_0, p_0) \in \mathbf{H}_{\mathbf{g}_D, \Gamma_D}^1(\Omega_0) \times L^2(\Omega_0)$ satisfies for all $(\mathbf{v}_0, q_0) \in \mathbf{H}_{\mathbf{0}, \Gamma_D}^1(\Omega_0) \times L^2(\Omega_0)$,

$$\begin{aligned} \int_{\Omega_0} \sigma(\mathbf{u}_0) : \varepsilon(\mathbf{v}_0) \, dx - \int_{\Omega} p_0 \nabla \cdot \mathbf{v}_0 \, dx &= \int_{\Omega_0} \mathbf{f} \cdot \mathbf{v}_0 \, dx + \int_{\Gamma_N \setminus \gamma} \mathbf{g} \cdot \mathbf{v}_0 \, ds + \int_{\gamma_0} \mathbf{g}_0 \cdot \mathbf{v}_0 \, ds, \\ - \int_{\Omega} q_0 \nabla \cdot \mathbf{u}_0 \, dx &= - \int_{\Omega} q_0 f_c \, dx. \end{aligned} \quad (22)$$

By Ladyzhenskaya-Babuška-Brezzi theorem, problem (22) is well-posed.

Remark 4.4 As for the Poisson problem, and even though this is rarely a choice in applications, the best possible choices for the defeatured problem data \mathbf{f} and f_c in F_n^k for $k = 1, \dots, N_f$ and \mathbf{g}_0 on γ_0 will be guided by Remark 4.5. We anticipate that the defeaturing error will be smaller if the defeatured problem data satisfy a conservation assumption of the solution flux in the positive and negative components of the features. I.e., if they verify for all $k = 1, \dots, N_f$,

$$\int_{\gamma_{0,p}^k} \mathbf{g}_0 \, ds = \int_{\gamma_p^k} \mathbf{g} \, ds + \int_{F_p^k} \mathbf{f} \, dx \quad \text{and} \quad \int_{\gamma_{0,n}^k} \mathbf{g}_0 \, ds = \int_{\gamma_n^k} \mathbf{g} \, ds - \int_{F_n^k} \mathbf{f} \, dx. \quad (23)$$

Now, for all $k = 1, \dots, N_f$, we need to extend the solution (\mathbf{u}_0, p_0) of (22) to \tilde{F}_p^k as discussed in Section 2.1, where \tilde{F}_p^k satisfies the properties given in (4). To do so, let us choose an L^2 -extension of the restriction $\mathbf{f}|_{F_p^k}$ and an L^2 -extension of the restriction $f_c|_{F_p^k}$ in $G_p^k := \tilde{F}_p^k \setminus \overline{F_p^k}$, that we still write \mathbf{f} and f_c by abuse of notation. Moreover, we assume that the viscous stress tensor σ also satisfies (17) on functions defined in \tilde{F}_p^k . Then we define for all $k = 1, \dots, N_f$ the following extension of the solution (\mathbf{u}_0, p_0) of (21) in \tilde{F}_p^k : after choosing $\tilde{\mathbf{g}}^k \in \mathbf{H}^{\frac{1}{2}}(\tilde{\gamma}^k)$, find $(\mathbf{u}_k, p_k) \in \mathbf{H}^1(\tilde{F}_p^k) \times L^2(\tilde{F}_p^k)$, the weak solution of

$$\mathcal{P}(\tilde{F}_p^k) : \begin{cases} -\nabla \cdot \sigma(\mathbf{u}_k) + \nabla p_k = \mathbf{f} & \text{in } \tilde{F}_p^k \\ \nabla \cdot \mathbf{u}_k = f_c & \text{in } \tilde{F}_p^k \\ \mathbf{u}_k = \mathbf{u}_0 & \text{on } \gamma_{0,p}^k \\ \sigma(\mathbf{u}_k)\tilde{\mathbf{n}}^k - p_k\tilde{\mathbf{n}}^k = \tilde{\mathbf{g}}^k & \text{on } \tilde{\gamma}^k \\ \sigma(\mathbf{u}_k)\tilde{\mathbf{n}}^k - p_k\tilde{\mathbf{n}}^k = \mathbf{g} & \text{on } \gamma_s^k, \end{cases} \quad (24)$$

that is, $(\mathbf{u}_k, p_k) \in \mathbf{H}_{\mathbf{u}_0, \gamma_{0,p}^k}^1(\tilde{F}_p^k) \times L^2(\tilde{F}_p^k)$ satisfies for all $(\mathbf{v}^k, q^k) \in \mathbf{H}_{\mathbf{0}, \gamma_{0,p}^k}^1(\tilde{F}_p^k) \times L^2(\tilde{F}_p^k)$,

$$\begin{aligned} \int_{\tilde{F}_p^k} \boldsymbol{\sigma}(\mathbf{u}_k) : \boldsymbol{\varepsilon}(\mathbf{v}^k) \, dx - \int_{\tilde{F}_p^k} p_k \boldsymbol{\nabla} \cdot \mathbf{v}^k \, dx &= \int_{\tilde{F}_p^k} \mathbf{f} \cdot \mathbf{v}^k \, dx + \int_{\tilde{\gamma}^k} \tilde{\mathbf{g}}^k \cdot \mathbf{v}^k \, ds + \int_{\gamma_s^k} \mathbf{g} \cdot \mathbf{v}^k \, ds, \\ - \int_{\tilde{F}_p^k} q^k \boldsymbol{\nabla} \cdot \mathbf{u}_k \, dx &= - \int_{\tilde{F}_p^k} q^k f_c \, dx. \end{aligned} \quad (25)$$

By Ladyzhenskaya-Babuška-Brezzi theorem, problem (25) is well-posed. The choice of the defeatured problem data \mathbf{f} and f_c in G_p^k , and $\tilde{\mathbf{g}}^k$ on $\tilde{\gamma}^k$ for $k = 1, \dots, N_f$ will be guided by Remark 4.5. We anticipate here that as before, the best possible choices satisfy a conservation assumption of the solution flux in every feature's extension G_p^k . I.e., they verify for all $k = 1, \dots, N_f$,

$$\int_{\tilde{\gamma}^k} \tilde{\mathbf{g}}^k \, ds = \int_{\gamma_r^k} \mathbf{g} \, ds - \int_{\tilde{F}_p^k \setminus F_p^k} \mathbf{f} \, dx. \quad (26)$$

Then, the defeatured solution $(\mathbf{u}_d, p_d) \in \mathbf{H}_{\mathbf{g}_D, \Gamma_D}(\Omega) \times L^2(\Omega)$ is defined from (\mathbf{u}_0, p_0) and (\mathbf{u}_k, p_k) for $k = 1, \dots, N_f$ as in (3) and we define the defeaturing error as

$$\|(\mathbf{u} - \mathbf{u}_d, p - p_d)\|_{\Omega} = \left(\int_{\Omega} \boldsymbol{\sigma}(\mathbf{u} - \mathbf{u}_d) : \boldsymbol{\varepsilon}(\mathbf{u} - \mathbf{u}_d) \, dx \right)^{\frac{1}{2}} + \mu^{-\frac{1}{2}} \|p - p_d\|_{0,\Omega}. \quad (27)$$

4.2 Defeating error estimator

Let us recall the definition of the defeatured solution (\mathbf{u}_d, p_d) from (3), and the definitions of Σ , Σ^k , Σ_n , $\Sigma_{0,p}$, and Σ_r from (6). Then for all $\gamma \in \Sigma$, let $k_{\gamma} \equiv k$ if $\gamma \in \Sigma^k$ for some $k = 1, \dots, N_f$, and let us redefine \mathbf{d}_{γ} for all $\gamma \in \Sigma$ in the context of Stokes equations. That is, let

$$\mathbf{d}_{\gamma} \equiv \begin{cases} \mathbf{g} - \boldsymbol{\sigma}(\mathbf{u}_d) \mathbf{n} + p_d \mathbf{n} & \text{if } \gamma \in \Sigma_n \text{ or if } \gamma \in \Sigma_r, \\ -(\mathbf{g}_0 + \boldsymbol{\sigma}(\mathbf{u}_d) \mathbf{n}^{k_{\gamma}} - p_d \mathbf{n}^{k_{\gamma}}) & \text{if } \gamma \in \Sigma_{0,p}. \end{cases} \quad (28)$$

In other words, and as for Poisson's equations, \mathbf{d}_{γ} represents the Neumann error on the boundaries γ_n and γ_r due to the defeaturing process, and the jump of the normal derivative of the defeatured solution on the boundaries $\gamma_{0,p}$. Then, we define the *a posteriori* defeaturing error estimator as:

$$\mathcal{E}(\mathbf{u}_d, p_d) := \left(\sum_{\gamma \in \Sigma} \mathcal{E}_{\gamma}(\mathbf{u}_d, p_d)^2 \right)^{\frac{1}{2}}, \quad (29)$$

where for all $\gamma \in \Sigma$,

$$\mathcal{E}_{\gamma}(\mathbf{u}_d, p_d) := \mu^{-\frac{1}{2}} \left(|\gamma|^{\frac{1}{n-1}} \|\mathbf{d}_{\gamma} - \overline{\mathbf{d}_{\gamma}}^{\gamma}\|_{0,\gamma}^2 + c_{\gamma}^2 |\gamma|^{\frac{n}{n-1}} \|\overline{\mathbf{d}_{\gamma}}^{\gamma}\|_{\ell^2}^2 \right)^{\frac{1}{2}}, \quad (30)$$

where $\overline{\mathbf{d}_{\gamma}}^{\gamma}$ is defined in (14), $\overline{\mathbf{d}_{\gamma}}^{\gamma}$ denotes the dimension-wise average value of \mathbf{d}_{γ} over γ , and $\|\cdot\|_{\ell^2}$ denotes the discrete ℓ^2 -norm as $\overline{\mathbf{d}_{\gamma}}^{\gamma} \in \mathbb{R}^n$. Note that, as for Poisson's problem, we can rewrite the estimator feature-wise as

$$\mathcal{E}(\mathbf{u}_d, p_d) = \left(\sum_{k=1}^{N_f} \sum_{\gamma \in \Sigma^k} \mathcal{E}_{\gamma}(\mathbf{u}_d, p_d)^2 \right)^{\frac{1}{2}} = \left(\sum_{k=1}^{N_f} \mathcal{E}^k(\mathbf{u}_d, p_d)^2 \right)^{\frac{1}{2}}, \quad (31)$$

where for all $k = 1, \dots, N_f$, we define $\mathcal{E}^k(\mathbf{u}_d, p_d)$ as the defeaturing error estimator for feature F^k , that is,

$$\mathcal{E}^k(\mathbf{u}_d, p_d) := \left(\sum_{\gamma \in \Sigma^k} \mathcal{E}_{\gamma}(\mathbf{u}_d, p_d)^2 \right)^{\frac{1}{2}}.$$

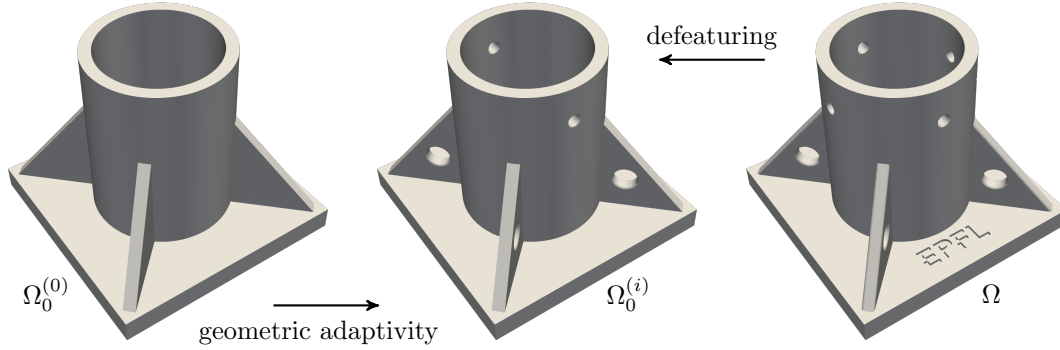


Figure 7: Illustration of defeaturing and geometric adaptivity.

The proposed estimator indicates that all the information on the error introduced by defeaturing is encoded in the boundary of the features, and can be accounted by suitably evaluating the error made on the normal viscous stress and pressure of the solution.

Remark 4.5 Similarly to Remark 3.2, the terms involving the component-wise average values of \mathbf{d}_γ in $\mathcal{E}(\mathbf{u}_d, p_d)$ only depend on the defeatured problem data. As a consequence, if these terms dominate, this means that the defeatured problem data should be more accurately chosen. Moreover, under the reasonable data compatibility conditions (23) and (26) that represent flux conservation assumptions in this context, the

defeating error estimator (29) rewrites $\mathcal{E}(\mathbf{u}_d, p_d) := \mu^{-\frac{1}{2}} \left(\sum_{\gamma \in \Sigma} |\gamma|^{\frac{1}{n-1}} \|\mathbf{d}_\gamma\|_{0,\gamma}^2 \right)^{\frac{1}{2}}$.

Remark 4.6 Similarly to Remark 3.3, note that

$$\mathcal{E}(\mathbf{u}_d, p_d) \lesssim \mu^{-\frac{1}{2}} \left(\sum_{\gamma \in \Sigma} c_\gamma^2 |\gamma|^{\frac{1}{n-1}} \|\mathbf{d}_\gamma\|_{0,\gamma}^2 \right)^{\frac{1}{2}} =: \tilde{\mathcal{E}}(\mathbf{u}_d, p_d).$$

However, when $n = 2$ and under the flux conservation conditions (23) and (26), $\tilde{\mathcal{E}}(\mathbf{u}_d, p_d)$ is sub-optimal since in this case, $\tilde{\mathcal{E}}(\mathbf{u}_d, p_d) \lesssim \max_{\gamma \in \Sigma} (c_\gamma) \mathcal{E}(\mathbf{u}_d, p_d)$.

Remark 4.7 If the linear elasticity equations are considered instead of Stokes' equations, with λ and μ denoting the Lamé coefficients, then the pressure terms in the Neumann error (28) should be removed, and the weight $\mu^{-\frac{1}{2}}$ in equation (30) should be replaced by $\rho^{-\frac{1}{2}}$, where $\rho = \mu$ if $\lambda \geq 0$, and $\rho = \min(\mu, \frac{3}{2}\lambda + \mu)$ otherwise. The coefficient ρ corresponds to the coercivity constant of the bilinear form $\mathfrak{a}(\cdot, \cdot)$, see Appendix A. Then equations (29) and (31) defining the estimator remain the same for the linear elasticity equations.

5 An adaptive geometric refinement strategy

In this section, we aim at defining an adaptive analysis-aware defeaturing strategy in a geometry Ω containing $N_f \geq 1$ distinct complex features. More precisely, starting from a fully defeatured geometry Ω_0 , we want to precisely define a strategy that determines when and which geometrical features need to be reinserted in the geometrical model, among those that have been removed by defeaturing. Note that the word *defeating* may be misleading when thinking of an adaptive strategy: The geometry Ω_0 in which the problem is actually

solved is (partially) defeatured, but the adaptive algorithm selects the features that need to be *added* to the geometrical model, in order to solve the differential problem up to a given accuracy. The concept of geometric adaptivity is illustrated in Figure 7.

In the sequel, we elaborate on each of the building blocks which compose one iteration of an iterative process:



To do so, let $i \in \mathbb{N}$ be the current iteration index of the adaptive geometric refinement strategy. For simplicity in this section, let us always write u_d the defeatured solution, even in the context of linear elasticity for which it should be \mathbf{u}_d , or in the context of Stokes equations for which it should be (\mathbf{u}_d, p_d) . To begin the process, let $\Omega_0^{(0)}$ be the fully defeatured geometry defined as in (2). That is, $\Omega_0^{(0)}$ is the domain in which all features of Ω are removed: Their positive component is cut out, and their negative component is filled with material. Since some features will be reinserted during the adaptive process, we denote $\Omega_0^{(i)}$ the simplified geometry at the i -th iteration, and in general, we use the upper index (i) to refer to objects at the same iteration. However, to alleviate the notation, we will drop the index (i) when it is clear from the context. In particular, we will write $\Omega_0 \equiv \Omega_0^{(i)}$.

5.1 Solve and Estimate

We first solve the defeatured problem (8)/(22) defined in the (partially) defeatured geometry Ω_0 . Then, we solve the local extension problem (10)/(25) for each feature having a non-empty positive component. We thus obtain the defeaturing solution $u_d \equiv u_d^{(i)}$ defined in (3), as an approximation of the exact solution u of (7)/(18) at iteration i . Then, the defeaturing error is estimated by $\mathcal{E}(u_d)$ defined in (15)/(29).

5.2 Mark

Recalling that $N_f \equiv N_f^{(i)}$ at the current iteration i , we select and mark some features $\{F^{k_m}\}_{k_m \in I_m} \subset \mathfrak{F}$ with $I_m \subset \{1, \dots, N_f^{(i)}\}$ to be added to the (partially) defeatured geometry $\Omega_0 \equiv \Omega_0^{(i)}$. To do so, we employ in the following a maximum strategy, but any other convergent marking technique such as the Dörfler strategy [34] could be used. That is, let us first recall definition (16)/(31) of the single feature contributions $\mathcal{E}^k(u_d)$ of the defeaturing error estimator $\mathcal{E}(u_d)$, for $k = 1, \dots, N_f$. Then, after choosing a marking parameter $0 < \theta \leq 1$, a feature F^{k_m} is marked, i.e., $k_m \in I_m$, if it verifies

$$\mathcal{E}^{k_m}(u_d) \geq \theta \max_{k=1, \dots, N_f} (\mathcal{E}^k(u_d)). \quad (32)$$

In other words, the set of marked features are the ones giving the most substantial contribution to the defeaturing error estimator. The smallest is θ , the more features are selected, and viceversa.

5.3 Refine

In this step, the defeatured geometry $\Omega_0^{(i)}$ is refined, meaning that the marked features $\{F^k\}_{k \in I_m}$ are inserted in the geometrical model. That is, the new partially defeatured geometrical model $\Omega_0^{(i+1)}$ at the next iteration is built as follows:

$$\Omega_0^{(i+\frac{1}{2})} = \Omega_0^{(i)} \setminus \bigcup_{k \in I_m} F_n^k, \quad (33)$$

$$\Omega_0^{(i+1)} = \text{int} \left(\overline{\Omega_0^{(i+\frac{1}{2})}} \cup \bigcup_{k \in I_m} \overline{F_p^k} \right). \quad (34)$$

And thus in particular,

$$\begin{aligned} F_n^{(i+1)} &:= F_n^{(i)} \setminus \overline{\bigcup_{k \in I_m} F_n^k}, & F_p^{(i+1)} &:= F_p^{(i)} \setminus \overline{\bigcup_{k \in I_m} F_p^k}, \\ \tilde{F}_p^{(i+1)} &:= \tilde{F}_p^{(i)} \setminus \overline{\bigcup_{k \in I_m} \tilde{F}_p^k}, & \Omega_\star^{(i+1)} &:= \Omega \setminus \overline{F_p^{(i+1)}}, \end{aligned}$$

and as in definition (2),

$$\Omega_0^{(i+1)} = \text{int} \left(\overline{\Omega_\star^{(i+1)}} \cup \overline{F_n^{(i+1)}} \right).$$

Once the mesh and the defeatured geometry have been refined, the modules SOLVE and ESTIMATE presented in Section 5.1 can be called again. To do so, we update Ω_0 as $\Omega_0^{(i+1)}$, define $N_f^{(i+1)} := N_f^{(i)} - \#I_m$, update the set of features \mathfrak{F} as $\mathfrak{F} \setminus \{F^k\}_{k \in I_m}$, and renumber the features from 1 to $N_f^{(i+1)}$. The adaptive loop is continued until a certain given tolerance on the error estimator $\mathcal{E}(u_d)$ is reached, or until the set \mathfrak{F} is empty, meaning that all the features have been added to the geometrical model.

Remark 5.1 Note that a more precise geometric refinement strategy could be performed since G_p^k can be seen as a negative feature of F_p^k whose simplified domain is \tilde{F}_p^k , for all $k = 1, \dots, N_f$. More precisely, one could consider separately the contributions to $\mathcal{E}^k(u_d)$ given by

- γ_n^k and $\gamma_{0,p}^k$, which indicate whether feature F^k should be added to the defeatured geometrical model Ω_0 ;
- γ_r^k , which indicates whether the negative feature G_p^k of F_p^k should be removed from the simplified positive component \tilde{F}_p^k of F^k .

However, since this adds an extra complexity without introducing new conceptual ideas, this strategy is not further developed in the remainder of this article.

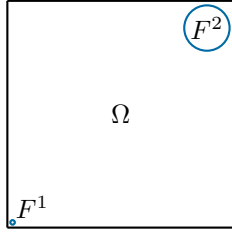
Remark 5.2 For a given a design, engineers often consider more than one set of boundary conditions, or in other words, they analyze the same design under different loading scenarios. Then, to decide whether the design is valid, they consider an envelope of the results thanks to a max-like function. The proposed adaptive strategy could be adapted to this context by computing the defeaturing error estimator (15)/(29) for each loading scenario. Then, one marks the union of the sets of features marked in each case, as the high-fidelity model used for the analysis should include the features that are important in all the considered loading scenarios.

6 Numerical considerations and experiments

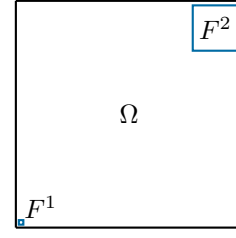
In this section, we perform a few numerical experiments to illustrate the validity of the proposed *a posteriori* estimators of the defeaturing error, introduced in Sections 3 and 4. Thanks to these experiments, we also demonstrate that the adaptive procedure presented in Section 5 ensures the convergence of the defeaturing error in the energy norm.

For the numerical approximation of the differential problems treated in this section, we use isogeometric analysis (IGA) on very fine meshes, and multipatch and unfitted boundary techniques for the geometrical description of the features. More specifically, a code has been developed on top of GeoPDEs [35], an open-source and free Octave/MATLAB package for the resolution of PDEs using IGA. The local meshing process required for the integration of trimmed elements uses the in-house tools presented in [36, 37], that have been linked to GeoPDEs. Finally, the 3D numerical experiment of Section 6.3 has been performed using an in-house C++ library for immersed problems that implements the folded decomposition technique presented in [38]. The interested reader is referred to [27] for a presentation of isogeometric analysis and advanced spline technologies.

It is important to remark that, even if in this work we adopted spline based discretizations, the estimator and methodology presented in this work are discretization agnostic, being possible to use other techniques.



(a) Exact domain with two circular features.



(b) Exact domain with two square features.

Figure 8: Numerical test 6.1.1 – Exact geometries used for the comparison between features’ sizes (not at scale).

| Features | $\mathcal{E}^1(u_0)$ | $\mathcal{E}^2(u_0)$ | $\mathcal{E}(u_0)$ | $\ u - u_d\ _\Omega$ | η_{eff} |
|----------------|----------------------|----------------------|----------------------|----------------------|---------------------|
| Circular holes | $5.03 \cdot 10^{-2}$ | $7.86 \cdot 10^{-6}$ | $5.03 \cdot 10^{-2}$ | $1.45 \cdot 10^{-2}$ | 3.47 |
| Square holes | $6.29 \cdot 10^{-2}$ | $7.73 \cdot 10^{-6}$ | $6.29 \cdot 10^{-2}$ | $1.64 \cdot 10^{-2}$ | 3.84 |

Table 1: Numerical test 6.1.1 – Results of the comparison between features’ sizes.

6.1 Impact of some feature properties on the defeaturing error

In this section, we study the impact of some properties of the geometrical features on the defeaturing error and estimator. In particular, we study the influence of the size and shape of the features, of the distance between them, and of their number.

6.1.1 Size of the features

Let us consider a numerical experiment first studied in [1], in which a computational domain contains a very small but important feature, and a large feature whose presence or absence does not affect much the solution accuracy. More precisely, let $\Omega_0 := (0, 1)^2$ be the fully defeatured geometry, and let $\Omega := \Omega_0 \setminus (F^1 \cup F^2)$, where F^1 is a circular hole of radius 10^{-3} centered at $(1.1 \cdot 10^{-3}, 1.1 \cdot 10^{-3})$, and F^2 is a larger circular hole of radius 10^{-1} centered at $(8.9 \cdot 10^{-1}, 8.9 \cdot 10^{-1})$. The considered geometry is illustrated in Figure 8a. We consider Poisson’s problem (7) in the exact computational domain Ω , and its defeatured version (8) defined in Ω_0 , with $f(x, y) := 128e^{-8(x+y)}$ in Ω_0 , $g_D(x, y) := e^{-8(x+y)}$ on $\Gamma_D := ([0, 1] \times \{0\}) \cup (\{0\} \times [0, 1])$, the bottom and left sides, $g(x, y) := -8e^{-8(x+y)}$ on $\partial\Omega_0 \setminus \overline{\Gamma_D}$, and finally $g \equiv 0$ on $\partial F^1 \cup \partial F^2$. The exact and defeatured solutions u and u_0 of these Poisson’s problems have a high gradient in the region around the small feature F^1 , while they are almost identically equal to zero in the region around the large feature F^2 .

We then perform the same test, but with square holes instead of circular ones. That is, we consider the same defeatured geometry $\Omega_0 = (0, 1)^2$, and the same data to solve Poisson’s equation (7), but now $\Omega := \Omega_0 \setminus (\overline{F^1} \cup \overline{F^2})$, where F^1 and F^2 are squares centered at $(1.1 \cdot 10^{-3}, 1.1 \cdot 10^{-3})$ and $(8.9 \cdot 10^{-1}, 8.9 \cdot 10^{-1})$, respectively, and whose sides have length $2 \cdot 10^{-3}$ and $2 \cdot 10^{-1}$, respectively. The geometry is illustrated in Figure 8b, and as before, the solution has a high gradient close to the bottom left corner where F^1 is located, and is almost constantly equal to zero close to the top right corner where F^2 is located.

The values of the defeaturing error estimator (15) and of the defeaturing error $\|u - u_d\|_\Omega$ are reported in Table 1. In both geometries, independently of the shape of the features, F^1 is indeed more important than F^2 since the estimator for F^1 is four orders of magnitude larger than the estimator for F^2 . This result was expected because of the solution’s very high gradient close to F^1 , and because of the homogeneous boundary conditions imposed on the feature’s boundaries. In both cases, the proposed estimator well estimates the defeaturing error since the effectivity index $\eta_{\text{eff}} := \frac{\mathcal{E}(u_0)}{\|u - u_d\|_\Omega}$ is reasonably low, with values comparable to the single feature experiments performed in [1]. These results perfectly agree with the theory developed in

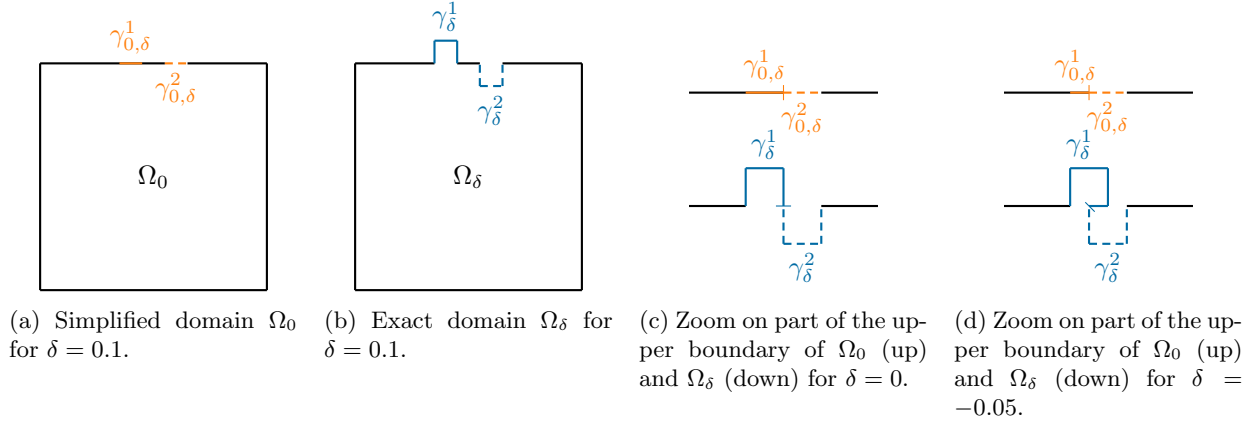


Figure 9: Numerical test 6.1.2 – Simplified domain Ω_0 and exact domains Ω_δ for different values of δ .

Section 3, and illustrate how the proposed estimator does not only depend on geometrical considerations, but also on the analysis behind, i.e., on the considered differential problem that one wants to solve. Hence the name *analysis-aware* defeaturing.

6.1.2 Distance between features

The following numerical example is used to show that the separability Assumption 2.1 is very weak, as one can consider features that are arbitrarily close to one another, as soon as the number of close features is bounded. Indeed, consider a geometry with either two square features, one positive and one negative, or one complex feature, as follows. Let $\Omega_0 := (0, 1)^2$, let $\delta \in (-0.1, 0.8)$, and let $\Omega_\delta := \text{int}(\overline{\Omega_0} \cup \overline{F_\delta^1} \setminus \overline{F_\delta^2})$ with

$$F_\delta^1 := \left(0.4 - \frac{\delta}{2}, 0.5 - \frac{\delta}{2}\right) \times (1, 1.1) \quad \text{and} \quad F_\delta^2 := \left(0.5 + \frac{\delta}{2}, 0.6 + \frac{\delta}{2}\right) \times (0.9, 1),$$

as illustrated in Figure 9. That is,

- if $\delta \leq 0$, then $F_\delta^1 \cup F_\delta^2$ needs to be considered as a single feature because of Assumption 2.1, where F_δ^1 is the positive component of that feature, and F_δ^2 is its negative component. In this case, we let $\gamma_{0,\delta}^1 := \gamma_{0,p}$, $\gamma_{0,\delta}^2 := \gamma_{0,n}$, $\gamma_\delta^1 := \gamma_p$, and $\gamma_\delta^2 := \gamma_n$;
- if $\delta > 0$, then F_δ^1 and F_δ^2 are two distinct features satisfying Assumption 2.1 and separated by a distance δ , where F_δ^1 is positive, and F_δ^2 is negative. In this case, we let $\gamma_{0,\delta}^1 := \gamma_{0,p}^1 = \gamma_0^1$, $\gamma_{0,\delta}^2 := \gamma_{0,n}^2 = \gamma_0^2$, $\gamma_\delta^1 := \gamma_p^1 = \gamma^1$, and $\gamma_\delta^2 := \gamma_n^2 = \gamma^2$.

Let us consider Poisson problem (7) with $f \equiv 0$ in Ω , $g_D(x, y) := 40 \cos(\pi x) + 10 \cos(5\pi x)$ on $\Gamma_D := (0, 1) \times \{0\}$, and $g \equiv 0$ on $\Gamma_N := \partial\Omega_\delta \setminus \overline{\Gamma_D}$. We solve the defeatured Poisson problem (8) with the same data, and we take $g_0 \equiv 0$ on

$$\gamma_{0,\delta}^1 = \left(0.4 - \frac{\delta}{2}, 0.5 - \frac{|\delta|}{2}\right) \times \{1\} \quad \text{and} \quad \gamma_{0,\delta}^2 = \left(0.5 + \frac{\delta}{2}, 0.6 + \frac{\delta}{2}\right) \times \{1\}.$$

Finally, we solve the Dirichlet extension problem (10) in $\tilde{F}_\delta^1 = F_\delta^1$. We choose different values of δ in order to consider different cases:

- with $\delta = 2 \cdot 10^{-1}$, the distance between the features and the distance between $\gamma_{0,\delta}^1$ and $\gamma_{0,\delta}^2$ are of the same order of magnitude as the measures of $\gamma_{0,\delta}^1$ and $\gamma_{0,\delta}^2$;

| δ | $\mathcal{E}(u_d)$ | $\ u - u_d\ _{\Omega_\delta}$ | η_{eff} |
|----------------------|--------------------|-------------------------------|---------------------|
| $2.0 \cdot 10^{-1}$ | 1.58 | 1.49 | 1.73 |
| $2.0 \cdot 10^{-4}$ | 2.84 | 1.68 | 1.69 |
| $0.0 \cdot 10^0$ | 2.84 | 1.68 | 1.69 |
| $-1.0 \cdot 10^{-3}$ | 27.0 | 15.1 | 1.78 |
| $-9.9 \cdot 10^{-2}$ | 24.5 | 14.3 | 1.71 |

Table 2: Numerical test 6.1.2 – Values of the defeaturing error and estimator for different values of δ . The cases in which $\delta > 0$ correspond to separate features, while the cases $\delta < 0$ correspond to features with overlapping boundaries.

- with $\delta = 2 \cdot 10^{-4}$, the distance between $\gamma_{0,\delta}^1$ and $\gamma_{0,\delta}^2$ is several orders of magnitude smaller than the measures of $\gamma_{0,\delta}^1$ and $\gamma_{0,\delta}^2$;
- with $\delta = 0$, the boundaries of the feature components intersect in one single point;
- with $\delta = -1 \cdot 10^{-3}$, the measure of the intersection between the boundaries of the feature components is several orders of magnitude smaller than the measures of the boundaries of the features;
- with $\delta = -9.9 \cdot 10^{-2}$, the measure of the intersection between the boundaries of the feature components is of the same order of magnitude as the measures of the boundaries of the features.

The results are presented in Table 2, and we indeed see that the defeaturing estimator approximates well the defeaturing error in all the different presented cases. In particular, we observe that the effectivity index $\eta_{\text{eff}} := \frac{\mathcal{E}(u_d)}{\|u - u_d\|_{\Omega}}$ is not influenced by the distance separating the positive and negative components of the feature(s). This confirms the fact that Assumption 2.1 is not very restrictive in practice.

6.1.3 Number of features

Under Assumption 2.1, the effectivity index of the defeaturing error estimator should not depend on the number of features that are present in the original geometry Ω . To verify this, let $\Omega_0 := (0,1)^2$ be the fully defeatured domain, and let $\Omega := \Omega_0 \setminus \bigcup_{k=1}^{N_f} \overline{F^k}$, where $N_f = 27$, and the features F^k are circular holes of random radii in the interval $(0, 0.01)$ which are randomly distributed in Ω_0 , under the condition that Assumption 2.1 is satisfied. For the sake of reproducibility, the values of the radii and centers of the features are reported in Table 3. The exact domain Ω with all the 27 features is represented in Figure 10a.

We want to find a good approximation of the solution of Poisson's problem (7) in Ω , whose exact solution is shown in Figure 10c, being $f(x, y) := -18e^{-3(x+y)}$ in Ω_0 , $g_D(x, y) := e^{-3(x+y)}$ on the bottom and left boundaries, i.e., on $\Gamma_D := ([0, 1] \times \{0\}) \cup (\{0\} \times [0, 1])$, $g(x, y) := -3e^{-3(x+y)}$ on $\partial\Omega_0 \setminus \overline{\Gamma_D}$, and $g \equiv 0$ on ∂F^k for $k = 1, \dots, N_f$. Thus we perform the adaptive algorithm introduced in Section 5 starting from the fully defeatured domain $\Omega_0^{(0)} := \Omega_0$, with marking parameter $\theta = 0.95$. I.e., at every iteration we include the 5% of the features whose error contributes the most. We recursively solve the partially defeatured problem (8) in $\Omega_0^{(i)}$ at each iteration $i \geq 0$, and we call $u_0^{(i)}$ its solution.

The results are presented in Figure 11, and the sets of added features at each iteration are the following: $\{1\}$, $\{2, 6\}$, $\{4, 16\}$, $\{8\}$, $\{3\}$, $\{5\}$, $\{13\}$, $\{12\}$, $\{17\}$, $\{22\}$, $\{11\}$, $\{10\}$, $\{15\}$, $\{23\}$, $\{24, 16\}$, $\{7\}$, $\{20, 27\}$, $\{18, 25\}$, $\{21\}$, $\{14\}$, $\{19, 9\}$. For instance, the error is divided by 10 when 9 out of the 27 features are inserted in the partially defeatured geometrical model, i.e., a third of total number of features; this happens at iteration $i = 7$, and $\Omega_0^{(7)}$ is represented in Figure 10b. On the other hand, features 19, 20, 24, and 25, that are placed near the right top corner, where the solution is gradient is very small, are only activated in the last iterations. We remark that the iteration index is directly linked to the number $N_f^{(i)}$ at each iteration i , that is, to the number of features that are still missing in the simplified geometrical model $\Omega_0^{(i)}$ with respect to

| Feature index k | 1 | 2 | 3 | 4 | 5 | 6 | 7 | 8 | 9 |
|--------------------------|------|------|------|------|------|------|------|------|------|
| Radius $[\cdot 10^{-2}]$ | 8.13 | 6.64 | 3.89 | 7.40 | 8.18 | 6.00 | 0.85 | 9.22 | 0.54 |
| Center $[\cdot 10^{-2}]$ | 0.98 | 2.84 | 5.46 | 7.16 | 8.99 | 0.67 | 3.12 | 4.95 | 7.06 |
| | 0.93 | 1.24 | 0.57 | 0.93 | 1.04 | 3.40 | 3.03 | 3.08 | 2.48 |
| Feature index k | 10 | 11 | 12 | 13 | 14 | 15 | 16 | 17 | 18 |
| Radius $[\cdot 10^{-2}]$ | 5.27 | 1.19 | 3.80 | 8.13 | 2.44 | 8.84 | 7.13 | 3.78 | 2.49 |
| Center $[\cdot 10^{-2}]$ | 8.86 | 0.67 | 3.28 | 5.01 | 7.44 | 8.93 | 1.10 | 2.44 | 5.45 |
| | 2.90 | 5.35 | 4.46 | 5.09 | 4.88 | 5.07 | 6.93 | 6.78 | 7.73 |
| Feature index k | 19 | 20 | 21 | 22 | 23 | 24 | 25 | 26 | 27 |
| Radius $[\cdot 10^{-2}]$ | 2.53 | 6.67 | 0.50 | 6.85 | 6.20 | 7.47 | 8.77 | 2.00 | 1.00 |
| Center $[\cdot 10^{-2}]$ | 7.27 | 9.21 | 0.22 | 3.26 | 5.01 | 7.06 | 8.99 | 4.00 | 1.00 |
| | 7.33 | 6.96 | 8.24 | 9.15 | 9.10 | 8.78 | 8.98 | 7.00 | 9.00 |

Table 3: Numerical test 6.1.3 – Data of the 27 circular features.

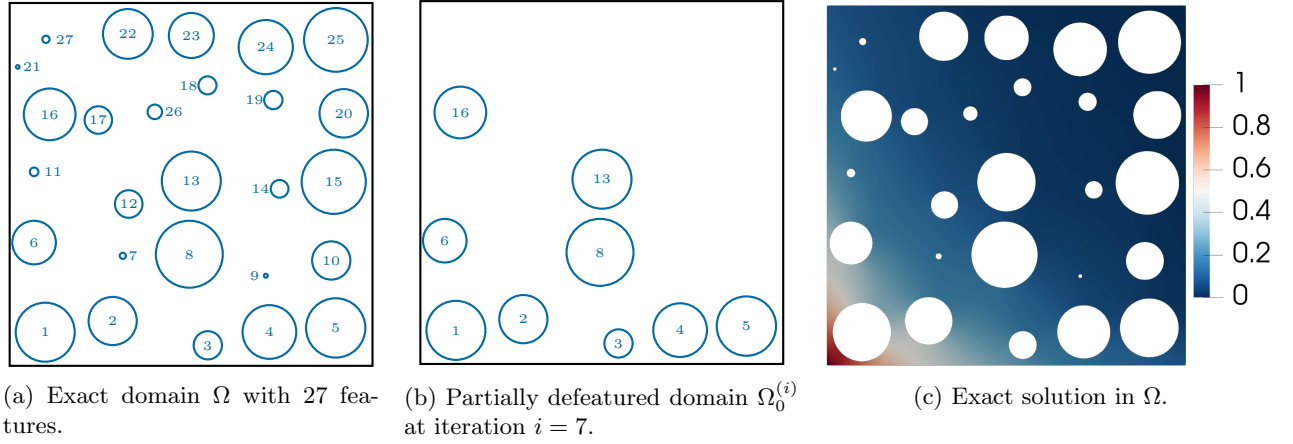


Figure 10: Numerical test 6.1.3 – Geometry with 27 features, considered exact solution, and corresponding partially defeatured geometrical model at iteration $i = 7$.

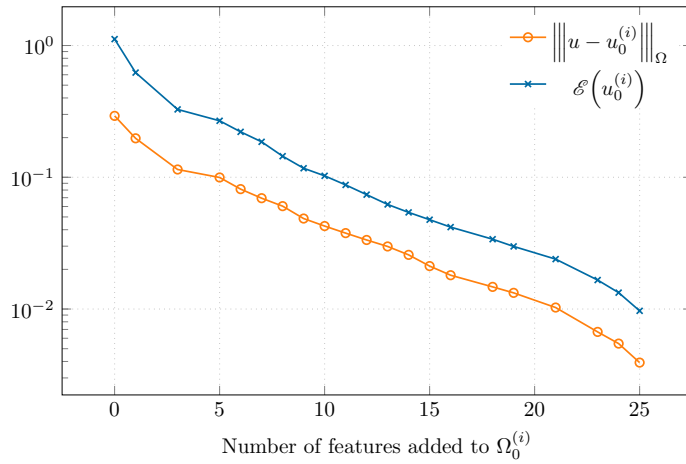


Figure 11: Numerical test 6.1.3 – Behavior of the defeaturing error and estimator with respect to the number of features in the defeatured geometrical models $\Omega_0^{(i)}$. Each marker corresponds to the value at one iteration.

| Feature index k | 1 | 2 | 3 |
|------------------------------------|------------------------|------------------------|------------------------|
| $\mathcal{E}^k(\mathbf{u}_d, p_d)$ | $2.1713 \cdot 10^{-2}$ | $2.4578 \cdot 10^{-2}$ | $1.5601 \cdot 10^{-2}$ |

Table 4: Numerical test 6.1.4 – Feature contributions $\mathcal{E}^k(\mathbf{u}_d, p_d)$ to the multi-feature estimator $\mathcal{E}(\mathbf{u}_d, p_d)$.

the 27 features in Ω . Moreover, we can see that the effectivity index is independent of the number of features that are not in the simplified geometrical model in which the problem is solved. Indeed, η_{eff} remains almost constant at each iteration, between 2.1 and 3.8. This result perfectly agrees with the theory developed in this paper, in particular the reliability and efficiency results of Theorems 2.5 and 2.7.

6.1.4 Shape of the features

The presence of a feature in the computational domain may greatly but locally perturb the solution, for instance because of a sharp or even re-entrant corner. When such feature is removed, the defeatured solution becomes smoother. In this section, the presented numerical illustration demonstrates that the proposed estimator is able to capture the correct behavior of the error independently of the shape of the feature, and with a low effectivity index.

To do so, let $\Omega_0 := (0, 1)^2$ be the fully defeatured domain, and let $\Omega := \Omega_0 \setminus \bigcup_{k=1}^3 \overline{F^k}$ be the exact computational domain containing three holes: F^1 is a circle of radius 0.0125 centered at (0.375, 0.5), F^2 is a square of side 0.0250 centered at (0.5, 0.375), and F^3 is a non-convex quadrilateral creating three re-entrant corners in Ω , whose vertices are placed in (0.625, 0.5125), (0.6125, 0.4875), (0.625, 0.5) and (0.6375, 0.4875). See Figure 12a (left) for an illustration of the domain Ω .

In this experiment, we aim at finding the exact solution (\mathbf{u}, p) of the Stokes' problem (18) defined in Ω , where $\mathbf{f}(x, y) := \exp[4((x - 0.5)^2 + (y - 0.5)^2)]$ and $f_c \equiv 0$ in Ω , $\mathbf{g}_D \equiv 0$ in $\partial\Omega_0$, and $\mathbf{g} \equiv 0$ in ∂F^k for all $k = 1, 2, 3$. Instead of solving problem (18), we tackle the approximate one (21) in Ω_0 with the same data; in particular, \mathbf{f} is naturally extended in the features, and we obtain the defeatured solution (\mathbf{u}_0, p_0) .

The magnitude of the velocity fields \mathbf{u} and \mathbf{u}_d is shown in Figure 12. As it can be seen in the zoom-in (Figure 12b), in this case, the sharp non-convex feature F^3 introduces a localized perturbation that is similar to ones produced by the sharp convex F^1 and smooth F^2 features, as all of them are located at solution regions with similar gradient magnitudes. Indeed, their contributions $\mathcal{E}^k(\mathbf{u}_d, p_d)$, for $k = 1, 2, 3$, reported in Table 4, are of the same order. From those individual contributions, through (31), the total defeaturing error estimate is computed to be $\mathcal{E}(\mathbf{u}_d, p_d) = 1.0895 \cdot 10^{-1}$, and the corresponding energy error is $\|(\mathbf{u} - \mathbf{u}_d, p - p_d)\|_{\Omega} = 7.5381 \cdot 10^{-2}$. Therefore, the effectivity index of the proposed estimator is

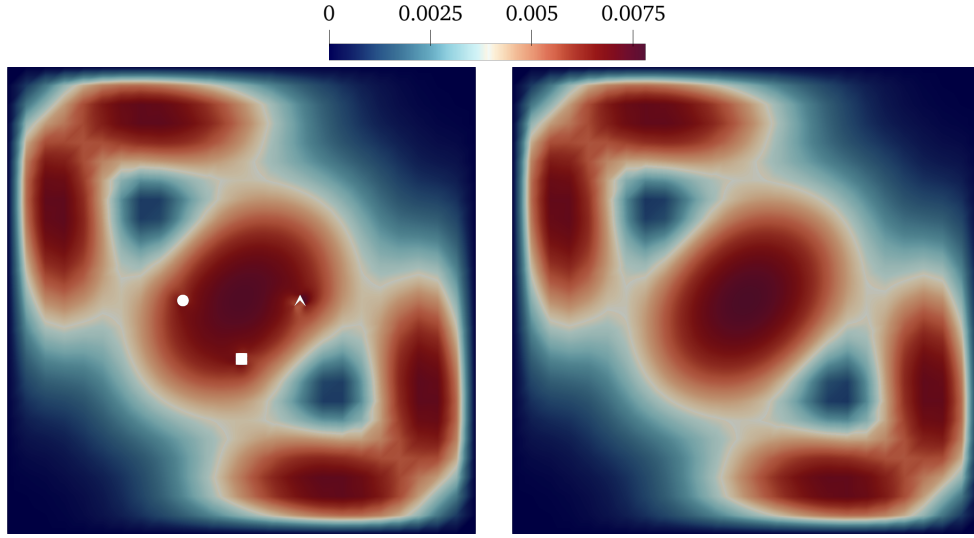
$$\eta_{\text{eff}} := \frac{\mathcal{E}(\mathbf{u}_d, p_d)}{\|(\mathbf{u} - \mathbf{u}_d, p - p_d)\|_{\Omega}} = 1.4454,$$

which is notably very low (at the same level as the ones observed in [1] for geometries with a single feature): The estimator is able to estimate the effect of different features, independently of their shape.

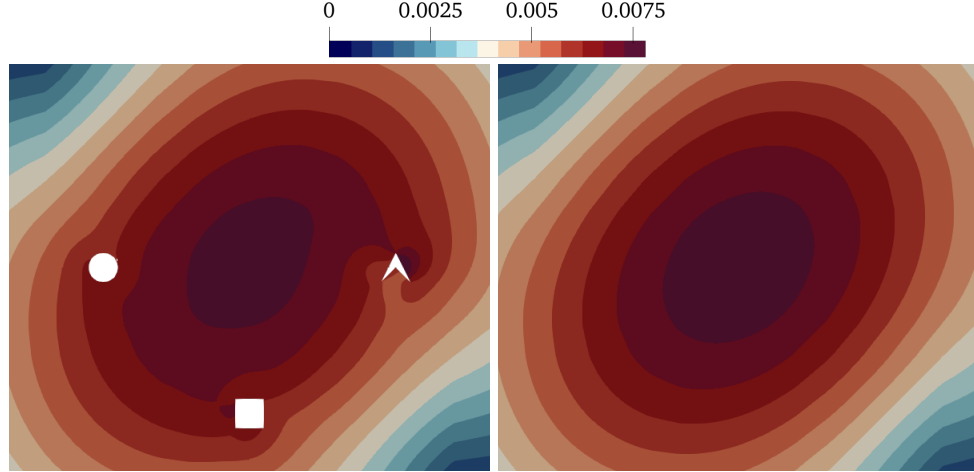
6.2 Lid-driven cavity

For this next numerical experiment, let us consider Stokes' problem in a lid-driven cavity [39] in which three holes are located. More precisely, we consider an exact domain $\Omega = \Omega_0 \setminus (\overline{F^1} \cup \overline{F^2} \cup \overline{F^3})$ for which $\Omega_0 := (0, 1)^2$ is the fully defeatured domain, and F^1 , F^2 , and F^3 are three circular holes of radius 0.01 centered, respectively, at (0.011, 0.989), (0.5, 0.75), and (0.011, 0.011). For this test, we let $\Gamma_D := \partial\Omega_0$, $\Gamma_N := \partial F^1 \cup \partial F^2 \cup \partial F^3$, $\mathbf{f} \equiv \mathbf{0}$ in Ω_0 , $\mathbf{g} \equiv \mathbf{0}$ on Γ_N , and

$$\mathbf{g}_D \equiv \begin{cases} (1, 0) & \text{on } (0, 1) \times \{1\} \text{ the top boundary,} \\ (0, 0) & \text{everywhere else on } \Gamma_D. \end{cases}$$



(a) Magnitude of \mathbf{u} (left) and \mathbf{u}_d (right) in the domains Ω and Ω_0 , respectively.



(b) Zoom of the central region: Magnitude of \mathbf{u} (left) and \mathbf{u}_d (right) in the domains Ω and Ω_0 , respectively.

Figure 12: Numerical test 6.1.4 – Magnitude of the velocity in the exact Ω and fully defeatured Ω_0 domains.

Then, let (\mathbf{u}, p) be the solution of the exact Stokes' problem (18), and let $(\mathbf{u}_d, p_d) \equiv (\mathbf{u}_0, p_0)$ be the solution of the corresponding Stokes' problem (21) in the fully defeatured geometry Ω_0 . We compute the estimator $\mathcal{E}(\mathbf{u}_d, p_d)$ defined in (31) by computing each feature contribution $\mathcal{E}^k(\mathbf{u}_d, p_d)$ for $k = 1, 2, 3$.

Results are presented in Figure 13, in which the magnitude of the velocity fields \mathbf{u} and \mathbf{u}_0 is shown, and Table 5 reports each feature contribution's $\mathcal{E}^k(\mathbf{u}_d, p_d)$ for $k = 1, 2, 3$. We observe that the presence of the features changes the fluid velocity inside the cavity, especially for features F^2 and F^3 . This is expected because of the homogeneous Neumann boundary conditions on the features. However, features only change locally the velocity field of the fluid around them. Thus, feature F^1 brings the largest contribution to the estimator while feature F^3 brings the smallest one. This is coherent with the theory since the velocity has a large gradient close to the moving boundary at the top, while it is almost constantly equal to zero around features F^2 and F^3 (note the different scales in Figures 13b-13d). We therefore expect F^1 to contribute the most to the overall defeaturing error, even if at a first glance it is the hole whose absence changes the least the velocity of the fluid (recall Figure 13b).

| Feature index k | 1 | 2 | 3 |
|------------------------------------|---------------------|------------------------|------------------------|
| $\mathcal{E}^k(\mathbf{u}_d, p_d)$ | $1.1874 \cdot 10^1$ | $6.7065 \cdot 10^{-2}$ | $2.1130 \cdot 10^{-2}$ |

Table 5: Numerical test 6.2 – Feature contributions $\mathcal{E}^k(\mathbf{u}_d, p_d)$ to the multi-feature estimator $\mathcal{E}(\mathbf{u}_d, p_d)$.

The total defeaturing error estimate is equal to $\mathcal{E}(\mathbf{u}_d, p_d) = 35.622$, and $\|(\mathbf{u} - \mathbf{u}_d, p - p_d)\|_\Omega = 31.308$. Therefore, the effectivity index of the proposed estimator is equal to

$$\eta_{\text{eff}} := \frac{\mathcal{E}(\mathbf{u}_d, p_d)}{\|(\mathbf{u} - \mathbf{u}_d, p - p_d)\|_\Omega} = 1.1378,$$

which is notably very low, as in the previous experiment. Note that to compute the defeaturing error, a very fine mesh around the holes had to be taken in Ω in order to be able to neglect the component of the error coming from the numerical approximation of the problem, as represented in Figure 14. This is not required when the holes are filled as in the defeatured geometry Ω_0 : This shows the potential of defeaturing, in terms of memory and computational time savings. Far from the features and high solution gradients, a coarser grid is considered.

6.3 Three-dimensional elastic structure

For this last numerical experiment, let us consider the exact domain Ω and the corresponding defeatured domain Ω_0 represented in Figure 15. More precisely, the base has dimensions $200 \times 200 \times 20$ [mm], and the cylinder has a height of 150 [mm]. Moreover, and in particular, the exact domain contains 20 features numbered as illustrated in Figure 15a:

- F^1 to F^4 are the four letters of the carved “EPFL” logo, in order (see also Figure 7 in which these features are more clearly visible).
- F^5 to F^8 are the four holes in the stiffeners, counted counter-clockwise beginning from the one on the left of the “EPFL” logo.
- F^9 to F^{12} are the four holes in the vertical part of the structure, counted counter-clockwise beginning from the one above the “EPFL” logo.
- F^{13} to F^{20} are the eight rounds present on the left and right diagonal angles of the stiffeners, counted counter-clockwise beginning from the left round of the stiffener on the left of the “EPFL” logo.

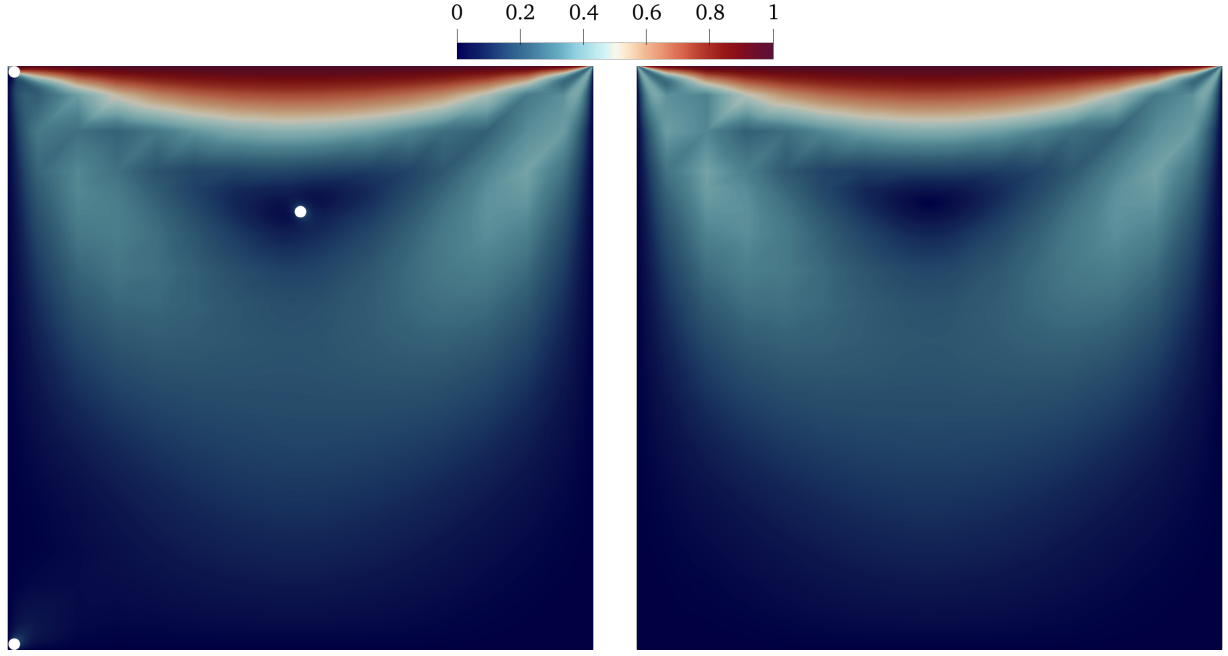
Rounds, holes, and carved logos are three of the most typical features that finite element analysis practitioners encounter in CAD designs. These features are interesting to analyze, since they are usual candidates to be removed before creating a finite element mesh.

Taking the origin at the bottom lower left corner of the structure, let Γ_D be the bottom of the structure and $\Gamma_N := \partial\Omega \setminus \overline{\Gamma_D}$, let $\mathbf{f} = \mathbf{0}$ [N · mm⁻³], $\mathbf{g}_D = \mathbf{0}$ [mm], and

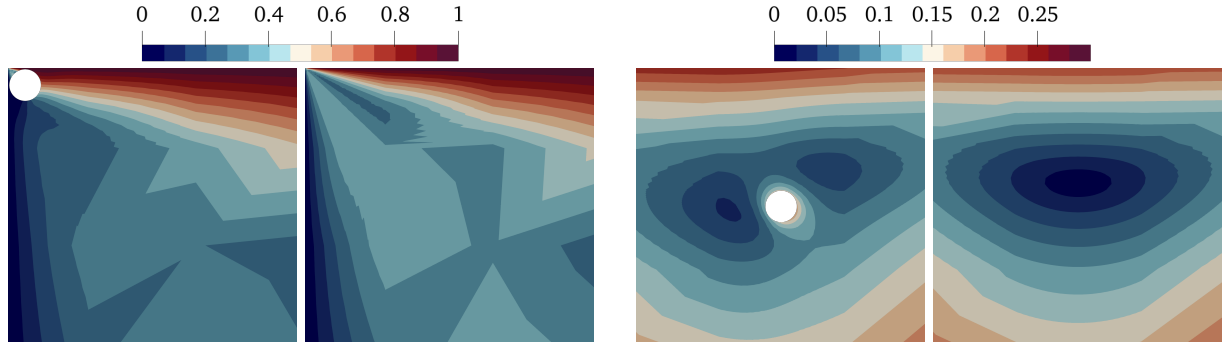
$$\mathbf{g} [\text{MPa}] = \begin{cases} \mathbf{0} & \text{on } \Gamma_N \setminus \overline{\Gamma_{\text{top}}} \\ \mathbf{e}_x = (1, 0, 0)^\top & \text{on } \Gamma_{\text{top}}, \end{cases}$$

where Γ_{top} is the top face of the cylinder. Then, let $\mathbf{u} \in \mathbf{H}_{0,\Gamma_D}^1(\Omega)$ be the solution of the linear elasticity problem given by (18) in which the pressure terms and the divergence condition are removed, and where the material properties correspond to steel. That is, the Lamé parameters λ and μ are expressed in terms of the Young modulus $E = 210$ [GPa] and Poisson’s ration $\nu = 0.3$ [–] as

$$\lambda = \frac{E\nu}{(1+\nu)(1-2\nu)} \quad \text{and} \quad \mu = \frac{E}{2(1+\nu)}.$$

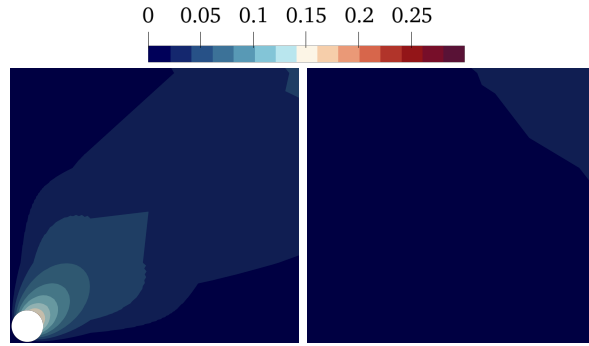


(a) Magnitude of \mathbf{u} (left) and \mathbf{u}_0 (right) in the domains Ω and Ω_0 , respectively.



(b) Magnitude of \mathbf{u} (left) and \mathbf{u}_0 (right) around F^1 .

(c) Magnitude of \mathbf{u} (left) and \mathbf{u}_0 (right) around F^2 .



(d) Magnitude of \mathbf{u} (left) and \mathbf{u}_0 (right) around F^3 .

Figure 13: Numerical test 6.2 – Magnitude of the velocity in the exact domain Ω and in the corresponding fully defeatured domain Ω_0 .

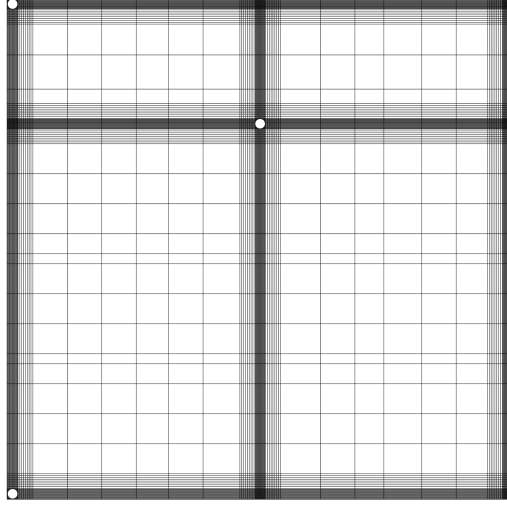


Figure 14: Numerical test 6.2 – Mesh used to compute an overkilled solution of the lid driven cavity Stokes’ problem in the exact domain Ω .

| Feature index k | 1 | 2 | 3 | 4 | 5 | 6 | 7 | 8 | 9 | 10 |
|--|-------|-------|-------|-------|-------|-------|-------|-------|-------|-------|
| $\mathcal{E}^k(\mathbf{u}_d)$ [$\cdot 10^{-8}$ J] | 1.949 | 2.904 | 3.032 | 1.278 | 69.28 | 69.28 | 69.28 | 69.24 | 61.96 | 26.06 |
| Feature index k | 11 | 12 | 13 | 14 | 15 | 16 | 17 | 18 | 19 | 20 |
| $\mathcal{E}^k(\mathbf{u}_d)$ [$\cdot 10^{-8}$ J] | 61.96 | 26.06 | 8.797 | 14.84 | 14.69 | 8.871 | 8.980 | 14.74 | 14.75 | 9.001 |

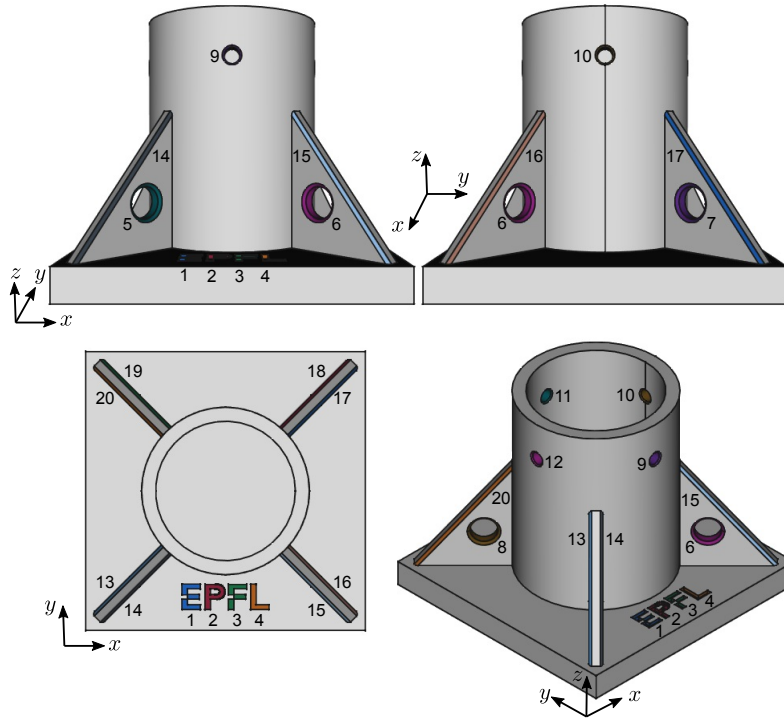
Table 6: Numerical test 6.3 – Feature contributions $\mathcal{E}^k(\mathbf{u}_d)$ to the multi-feature estimator $\mathcal{E}(\mathbf{u}_d)$.

Now, let us extend \mathbf{f} by $\mathbf{0}$ in all features so that $\mathbf{f} = \mathbf{0}$ [$\text{N} \cdot \text{m}^{-3}$] in Ω_0 , and let $\mathbf{g}_0 = \mathbf{0}$ [Pa] on $\gamma_0 := \partial\Omega_0 \setminus \overline{\partial\Omega}$. Then we compute the defeatured solution $\mathbf{u}_d \equiv \mathbf{u}_0 \in \mathbf{H}_{0,\Gamma_D}^1(\Omega_0)$ given by problem (22) in which again the pressure terms and the divergence condition are removed. Finally, we compute the estimator $\mathcal{E}(\mathbf{u}_d)$ defined in (31) with $p_d \equiv 0$ by computing each feature contribution $\mathcal{E}^k(\mathbf{u}_d)$ for $k = 1, \dots, 20$.

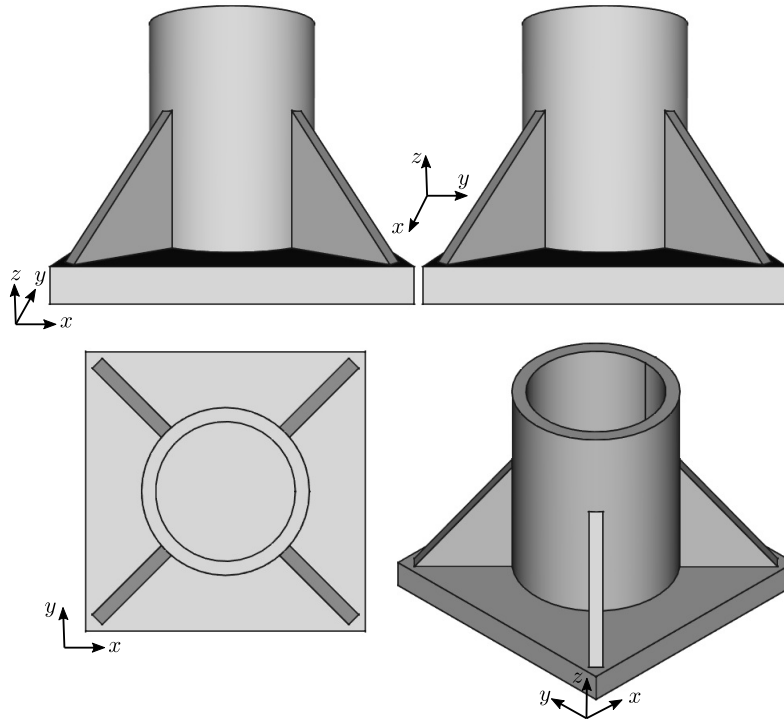
A rather fine mesh is used in order to reduce the error derived from numerical approximation. More precisely, the bounding box of Ω_0 is meshed with $n_{\text{el}} = 128$ elements per direction, and B-splines of degree 2 and regularity 1 are used. Results are presented in Table 6, where we report each feature’s contribution $\mathcal{E}^k(\mathbf{u}_d)$ for $k = 1, \dots, 20$. The obtained total error estimator is equal to $\mathcal{E}(\mathbf{u}_d) = 1.716 \cdot 10^{-6}$ [J]. Moreover, the magnitude of the solution displacements \mathbf{u} and \mathbf{u}_d , and the corresponding von Mises stress distributions are shown in Figures 16 and 17, respectively.

We can first see that the absence of features F^5 to F^8 in the defeatured geometry significantly affects the solution in the stiffeners. This is indeed reflected in the estimator: The estimator contributions of those four features is very large, corresponding to around half of the total error estimator. On the other hand, the solution is basically constant around the “EPFL” logo, no deformation is observed around it. We can therefore expect that the absence of features F^1 to F^4 in the defeatured geometry is not affecting much the accuracy of the solution. This is indeed observed in the estimator contributions of those features, as $\mathcal{E}^1(\mathbf{u}_d)$ to $\mathcal{E}^4(\mathbf{u}_d)$ are the lowest contributions of the estimator, corresponding to around 1% – 2% of $\mathcal{E}(\mathbf{u}_d)$. This is a typical situation that simulation practitioners encounter daily: Carved logos and trademarks are usually defeatured before creating a finite element mesh, since they complicate the meshing process and increase the number of elements (see, e.g., Figure 1a), but they contribute little to the accuracy of the problem’s solution. The proposed estimator identifies them straightaway.

Let us now run the adaptive algorithm introduced in Section 5 with $\theta = 0.99$ as marking parameter, until all features are added to the geometrical model. We call $\mathbf{u}_d^{(i)}$ the solution of the defeatured problem at



(a) Exact geometry Ω and numbering of the 20 features (in color).



(b) Defeatured geometry Ω_0

Figure 15: Numerical test 6.3 – Exact and defeatured 3D domains; the colored boundaries correspond to γ^k , for each feature $k = 1, \dots, 20$ as numbered in (a).

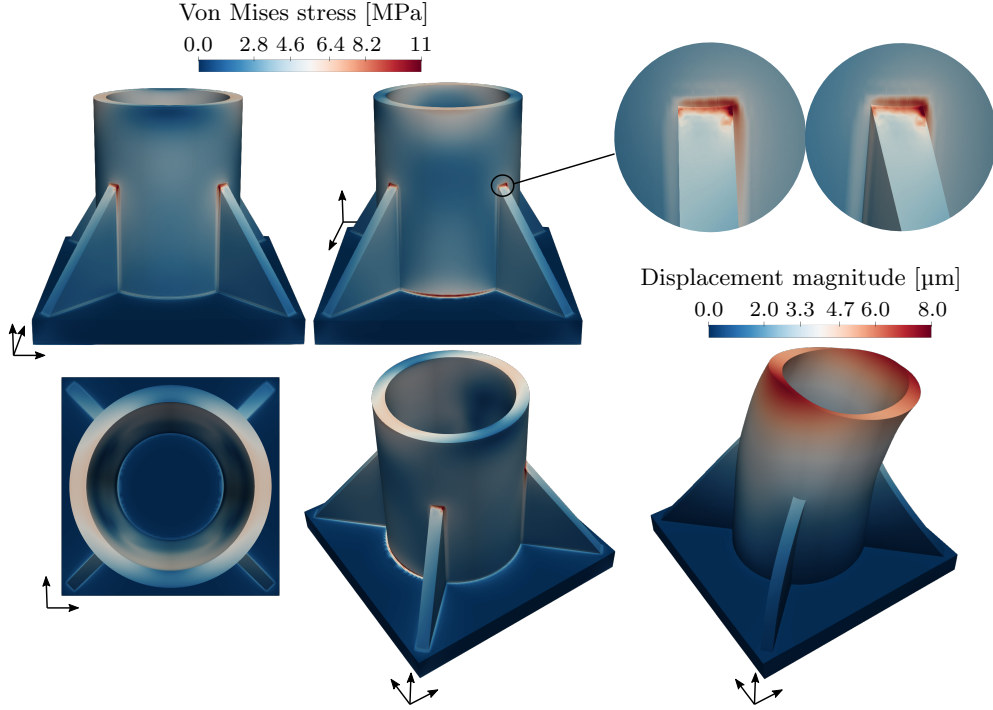


Figure 16: Numerical test 6.3 – Defeatured solution in the defeatured geometry Ω_0 . The views correspond to those of Figure 15, and the deformed configuration is magnified $[\times 5 \cdot 10^3]$ for visualization purposes.

iteration i . In Table 7, we report the indices of the features that are added to the defeatured geometrical model at each iteration, together with the value of the estimator $\mathcal{E}(\mathbf{u}_d^{(i)})$. The magnitude of the solution displacement and the corresponding von Mises stress distribution at iteration 4 are represented in Figure 18. Comparing the values of the estimator at each iteration and the von Mises stress distributions around each feature, we can see that the features that are added to the geometrical model at each iteration seem to be the ones that are affecting the most the solution accuracy, as one would expect. In Table 7 we can also see that to reduce the error estimator by 90%, it is enough to consider 12 out of the total 20 features of Ω (see iteration 4, whose solution is represented in Figure 18).

For instance, the holes F^9 and F^{11} are added before the holes F^{10} and F^{12} during the adaptive process, because of the direction in which the structure is bending due to the applied traction along the x -direction; this is reflected by the variation of the von Mises stresses that are larger in F^9 and F^{11} than in F^{10} and F^{12} . We can also see that larger stresses are present nearer the rounds F^{14} , F^{15} , F^{18} , and F^{19} than around the other four rounds. This is again coming from the direction of the bending. And very interestingly, the estimator is able to capture this effect, as rounds F^{14} , F^{15} , F^{18} , and F^{19} are introduced in the defeatured geometry after iteration 3, while the other rounds are introduced later, after iterations 4 and 5. See, for instance, the stress distribution in the connection between features F^{17} and F^{18} and the main cylinder (zoom-in regions in Figures 16, 17, and 18). As it can be appreciated, the stress concentration is higher around feature F^{18} , fact that also reveals the estimator value in Table 6, and the fact that feature F^{18} is activated before than F^{17} (see Table 8 and Figure 18).

Rounds are other typical examples of features that are candidates to be removed. However, in this case, the situation is usually less clear. Indeed, on the one hand, rounds complicate the meshing process and increase the number of elements in the model. But on the other hand, depending on the boundary conditions, removing rounds may lead to the creation of singularities in the solution. The proposed estimator is able to determine the impact of removing those rounds.

Finally, the numerical error is not considered in this article. However, it is interesting to note that the

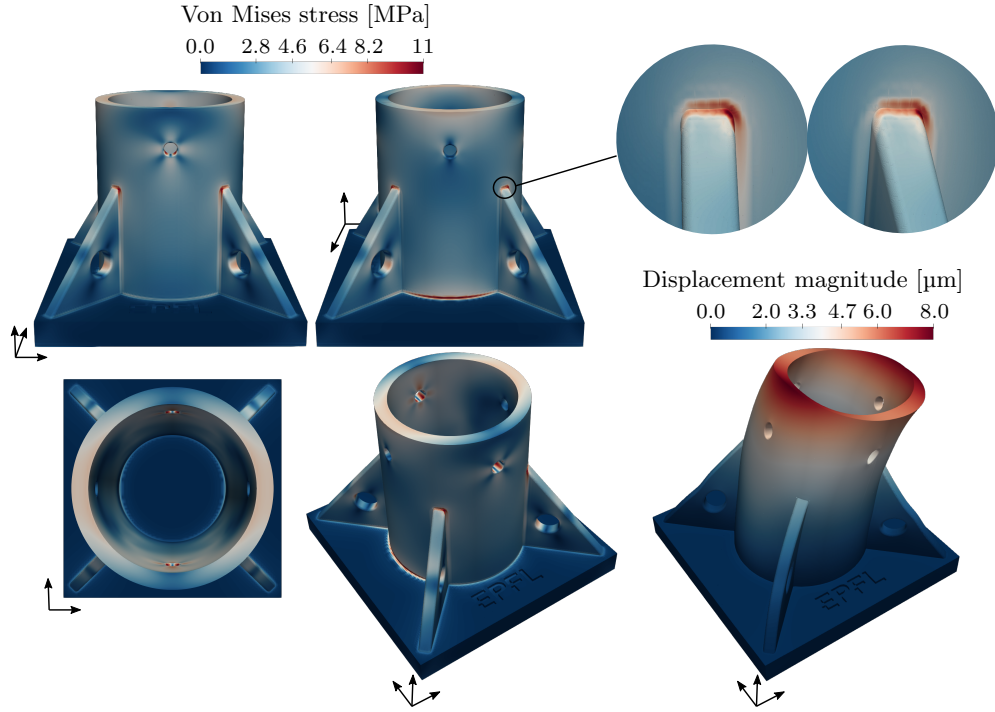


Figure 17: Numerical test 6.3 – Exact solution in the exact geometry Ω . The views correspond to those of Figure 15, and the deformed configuration is magnified $[\times 5 \cdot 10^3]$ for visualization purposes.

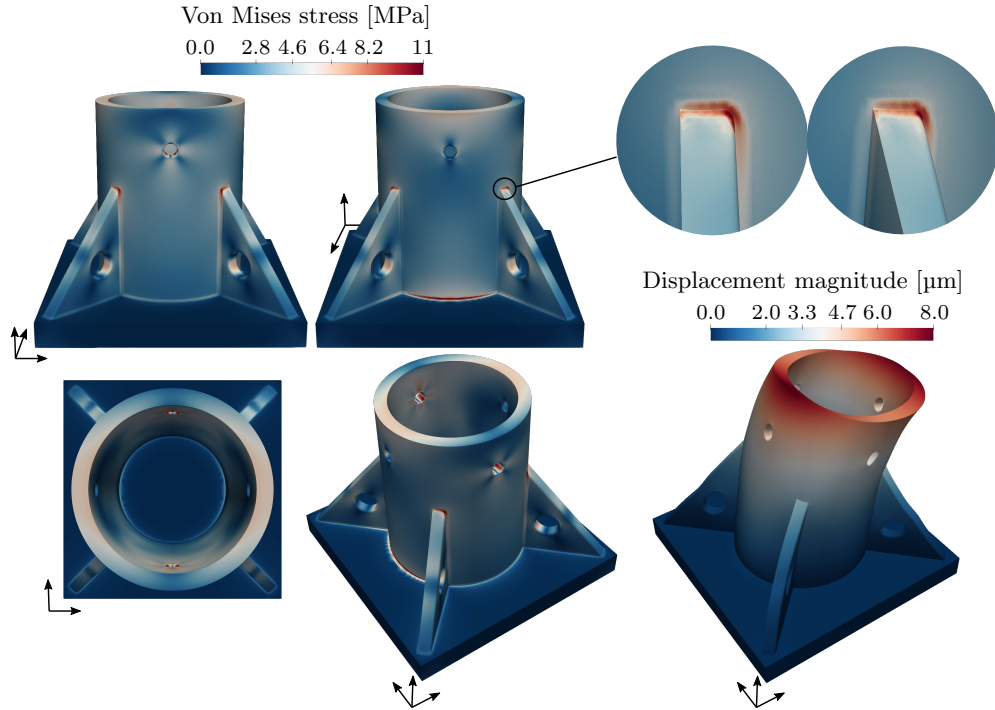


Figure 18: Numerical test 6.3 – Partially defeatured solution in the partially defeatured geometry obtained at iteration 4. The letters of the “EPFL” logo and the four rounds F^{13} , F^{16} , F^{17} , and F^{20} are the missing features in this geometry. The views correspond to those of Figure 15, and the deformed configuration is magnified $[\times 5 \cdot 10^3]$ for visualization purposes.

| Iteration i | 0 | 1 | 2 | 3 | 4 |
|--|------------|-------|--------|----------------|--------|
| Marked features | 5, 6, 7, 8 | 9, 11 | 10, 12 | 14, 15, 18, 19 | 17, 20 |
| $\mathcal{E}(\mathbf{u}_d^{(i)}) [\cdot 10^{-8} \text{J}]$ | 171.6 | 99.75 | 49.19 | 32.08 | 16.64 |
| Iteration i | 5 | 6 | 7 | 8 | 9 |
| Marked features | 13, 16 | 3 | 2 | 1 | 4 |
| $\mathcal{E}(\mathbf{u}_d^{(i)}) [\cdot 10^{-8} \text{J}]$ | 12.21 | 5.056 | 3.958 | 2.516 | 1.345 |

Table 7: Numerical test 6.3 – Results of the adaptive defeaturing strategy for $n_{\text{el}} = 128$ elements.

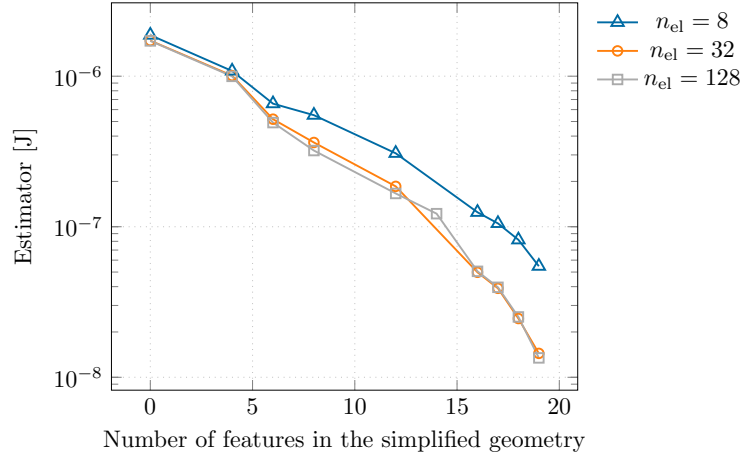


Figure 19: Numerical test 6.3 – Results of the adaptive defeaturing strategy for different discretization parameters.

| Iteration i | 0 | 1 | 2 | 3 | 4 | 5 | 6 | 7 | 8 | 9 |
|-----------------------|------------|-------|--------|----------------|----------------|--------|---|---|---|----------|
| $n_{\text{el}} = 8$ | 5, 6, 7, 8 | 9, 11 | 10, 12 | 14, 15, 18, 19 | 13, 16, 17, 20 | 1 | 2 | 3 | 4 | \times |
| $n_{\text{el}} = 32$ | 5, 6, 7, 8 | 9, 11 | 10, 12 | 14, 15, 18, 19 | 13, 16, 17, 20 | 3 | 2 | 1 | 4 | \times |
| $n_{\text{el}} = 128$ | 5, 6, 7, 8 | 9, 11 | 10, 12 | 14, 15, 18, 19 | 17, 20 | 13, 16 | 3 | 2 | 1 | 4 |

Table 8: Numerical test 6.3 – Marked features at each iteration on different mesh refinements.

estimator is still able to drive the proposed adaptive strategy on a coarser mesh. Indeed, this algorithm has been performed on multiple meshes containing a different number n_{el} of elements in each space direction of the bounding box of Ω_0 . More precisely, we have considered $n_{\text{el}} = 8, 32$, and 128 . In all three cases, the convergence of the estimator $\mathcal{E}(\mathbf{u}_d^{(i)})$ is reported in Figure 19, and the features chosen at each iteration are reported in Table 8. We can observe that except for features whose error contributions are very close to one another, the adaptive algorithm is able to correctly choose the important features, even on the coarsest mesh.

7 Conclusions

In the context of the Poisson’s, linear elasticity, and Stokes equations, we have studied the accuracy impact of removing distinct Neumann features from geometries in which the solution of a PDE is sought. In particular, we have generalized the *a posteriori* estimator of the energy norm of the defeaturing error from [1] to two- and three-dimensional geometries containing an arbitrary number of negative, positive, or generally complex features. The proposed estimator has the following properties:

- it is not only driven by geometrical considerations, but also by the PDE at hand;
- it is able to weight the impact of defeaturing in the energy norm, and its effectivity index is independent of the size of the geometrical features and of their number;
- it is able to determine whether the defeaturing error comes from the choice of defeaturing data (right hand side and Neumann boundary conditions), or if it comes from the importance of the presence of the feature itself;
- it is rigorously proven to be reliable and efficient up to oscillations;
- it is naturally decomposed into single feature contributions;
- it is simple, computationally cheap, and embarrassingly parallel, as it only requires the evaluation of fluxes through boundary pieces and the resolution of small problems at feature level.
- it has been tested on an extensive set of numerical experiments: In all of them, the estimator acts as an excellent approximation of the defeaturing error.

Note however that our framework does not include the case of a geometry whose boundary is complex everywhere as considered for instance in [29–31], because of Assumption 2.1.

Then, with the help of the proposed error estimator, we have been able to design an adaptive geometric refinement strategy taking into account the defeaturing errors. More precisely, starting from a fully defeatured geometry, features are iteratively added to the geometrical model when their absence is responsible for most of the solution accuracy loss. That is, the strategy is able to build a (partially) defeatured geometric model containing few features, for which the defeaturing error is below a prescribed tolerance. Presented numerical experiments have demonstrated the convergence of the defeaturing error during the adaptive loop. In a subsequent work [23], the proposed adaptive strategy will be combined with a mesh refinement strategy in the case in which a finite element method (and in particular isogeometric analysis [27, 28]) is used to approximately solve the PDE at hand.

Acknowledgments

The authors acknowledge the support of the European Research Council, via the ERC AdG project CHANGE n.694515. Pablo Antolín also acknowledges the support of the Swiss National Science Foundation through the project “Design-through-Analysis (of PDEs): the litmus test” n.40B2-0 187094 (BRIDGE Discovery 2019). Ondine Chanon also acknowledges the support of the Swiss National Science Foundation through the project n.P500PT_210974. Prof. Annalisa Buffa and Dr. Rafael Vázquez are also gratefully acknowledged for the fruitful discussions on the subject.

Declarations

Conflict of interest The authors declare that they have no conflict of interest.

References

- [1] A. Buffa, O. Chanon, and R. Vázquez, “Analysis-aware defeaturing: problem setting and *a posteriori* estimation,” *Mathematical Models and Methods in Applied Sciences*, vol. 32, no. 02, pp. 359–402, 2022.
- [2] J. Qian and Y. Zhang, “Automatic unstructured all-hexahedral mesh generation from B-Reps for non-manifold CAD assemblies,” *Engineering with Computers*, vol. 28, pp. 345–359, 2012.
- [3] D. R. White, S. Saigal, and S. J. Owen, “Meshing complexity of single part CAD models,” in *International Meshing Roundtable Conference*, pp. 121–134, Citeseer, 2003.
- [4] K. Lee, C. G. Armstrong, M. A. Price, and J. Lamont, “A small feature suppression/unsuppression system for preparing B-rep models for analysis,” in *Proceedings of the 2005 ACM symposium on Solid and Physical Modeling*, pp. 113–124, 2005.
- [5] C. Geuzaine and J.-F. Remacle, “Gmsh: A 3-D finite element mesh generator with built-in pre-and post-processing facilities,” *International Journal for Numerical Methods in Engineering*, vol. 79, no. 11, pp. 1309–1331, 2009.
- [6] R. Ferrandes, P. Marin, J.-C. Léon, and F. Giannini, “*A posteriori* evaluation of simplification details for finite element model preparation,” *Computers & Structures*, vol. 87, no. 1, pp. 73 – 80, 2009.
- [7] K. K. Choi and N.-H. Kim, *Structural Sensitivity Analysis and Optimization 1: Linear Systems*. Springer Science & Business Media, 2005.
- [8] J. Sokolowski and A. Zochowski, “On the topological derivative in shape optimization,” *SIAM Journal on Control and Optimization*, vol. 37, no. 4, pp. 1251–1272, 1999.
- [9] S. H. Gopalakrishnan and K. Suresh, “A formal theory for estimating defeaturing-induced engineering analysis errors,” *Computer-Aided Design*, vol. 39, no. 1, pp. 60–68, 2007.
- [10] S. H. Gopalakrishnan and K. Suresh, “Feature sensitivity: a generalization of topological sensitivity,” *Finite Elements in Analysis and Design*, vol. 44, no. 11, pp. 696–704, 2008.
- [11] I. Turevsky, S. H. Gopalakrishnan, and K. Suresh, “An efficient numerical method for computing the topological sensitivity of arbitrary-shaped features in plate bending,” *International Journal for Numerical Methods in Engineering*, vol. 79, no. 13, pp. 1683–1702, 2009.
- [12] J. Tang, S. Gao, and M. Li, “Evaluating defeaturing-induced impact on model analysis,” *Mathematical and Computer Modelling*, vol. 57, no. 3, pp. 413–424, 2013.
- [13] M. Li, S. Gao, and R. R. Martin, “Estimating the effects of removing negative features on engineering analysis,” *Computer-Aided Design*, vol. 43, no. 11, pp. 1402–1412, 2011. Solid and Physical Modeling 2011.
- [14] M. Li and S. Gao, “Estimating defeaturing-induced engineering analysis errors for arbitrary 3D features,” *Computer-Aided Design*, vol. 43, no. 12, pp. 1587–1597, 2011.
- [15] M. Li, S. Gao, and K. Zhang, “A goal-oriented error estimator for the analysis of simplified designs,” *Computer Methods in Applied Mechanics and Engineering*, vol. 255, pp. 89–103, 2013.
- [16] M. Li, S. Gao, and R. R. Martin, “Engineering analysis error estimation when removing finite-sized features in nonlinear elliptic problems,” *Computer-Aided Design*, vol. 45, no. 2, pp. 361–372, 2013.

- [17] J. T. Oden and S. Prudhomme, “Estimation of modeling error in computational mechanics,” *Journal of Computational Physics*, vol. 182, no. 2, pp. 496–515, 2002.
- [18] J. T. Oden and K. Vemaganti, “Estimation of local modeling error and goal-oriented adaptive modeling of heterogeneous materials: I. Error estimates and adaptive algorithms,” *Journal of Computational Physics*, vol. 164, no. 1, pp. 22–47, 2000.
- [19] C. Carstensen and S. Sauter, “A *posteriori* error analysis for elliptic PDEs on domains with complicated structures,” *Numerische Mathematik*, vol. 96, no. 4, pp. 691–721, 2004.
- [20] K. Vemaganti, “Modelling error estimation and adaptive modelling of perforated materials,” *International Journal for Numerical Methods in Engineering*, vol. 59, no. 12, pp. 1587–1604, 2004.
- [21] S. Repin, S. Sauter, and A. Smolianski, “A *posteriori* error estimation for the Dirichlet problem with account of the error in the approximation of boundary conditions,” *Computing*, vol. 70, no. 3, pp. 205–233, 2003.
- [22] S. Repin and S. Sauter, *Accuracy of mathematical models: dimension reduction, homogenization, and simplification*, vol. 33 of *EMS Tracts in Mathematics*. European Mathematical Society, Zürich, 2020.
- [23] A. Buffa, O. Chanon, and R. Vázquez, “Adaptive analysis-aware defeaturing,” *arXiv preprint arXiv:2212.05183*, 2022+.
- [24] O. Chanon, *Adaptive analysis-aware defeaturing*. PhD thesis, EPFL, 2022.
- [25] W. Hackbusch and S. Sauter, “Composite finite elements for the approximation of PDEs on domains with complicated micro-structures,” *Numerische Mathematik*, vol. 75, no. 4, pp. 447–472, 1997.
- [26] W. Hackbusch and S. Sauter, “Composite finite elements for problems containing small geometric details,” *Computing and Visualization in Science*, vol. 1, no. 1, pp. 15–25, 1997.
- [27] J. A. Cottrell, T. J. R. Hughes, and Y. Bazilevs, *Isogeometric analysis: towards integration of CAD and FEA*. Wiley, 2009.
- [28] T. J. R. Hughes, J. A. Cottrell, and Y. Bazilevs, “Isogeometric analysis: CAD, finite elements, NURBS, exact geometry, and mesh refinement,” *Computer Methods in Applied Mechanics and Engineering*, vol. 194, pp. 4135–4195, 2005.
- [29] A. Buffa, H. Ralf, and P. Panchal, “Adaptive approximation of shapes,” *Numerical Functional Analysis and Optimization*, vol. 42, no. 2, pp. 132–154, 2021.
- [30] T. Heydarov, A. Buffa, and B. Jüttler, “An unrefinement algorithm for planar THB-spline parameterizations,” *Computer Aided Geometric Design*, p. 102157, 2022.
- [31] J. Hinz, O. Chanon, A. Arrigoni, and A. Buffa, “A shape derivative approach to domain simplification,” *arXiv preprint arXiv:2306.05384*, 2023+.
- [32] A. Thakur, A. G. Banerjee, and S. K. Gupta, “A survey of CAD model simplification techniques for physics-based simulation applications,” *Computer-Aided Design*, vol. 41, no. 2, pp. 65–80, 2009.
- [33] D. Boffi, F. Brezzi, M. Fortin, *et al.*, *Mixed finite element methods and applications*, vol. 44. Springer, 2013.
- [34] W. Dörfler, “A convergent adaptive algorithm for Poisson’s equation,” *SIAM Journal on Numerical Analysis*, vol. 33, no. 3, pp. 1106–1124, 1996.
- [35] R. Vázquez, “A new design for the implementation of isogeometric analysis in Octave and Matlab: GeoPDEs 3.0,” *Computers & Mathematics with Applications*, vol. 72, no. 3, pp. 523–554, 2016.

- [36] P. Antolín, A. Buffa, and M. Martinelli, “Isogeometric analysis on V-reps: first results,” *Computer Methods in Applied Mechanics and Engineering*, vol. 355, pp. 976–1002, 2019.
- [37] X. Wei, B. Marussig, P. Antolín, and A. Buffa, “Immersed boundary-conformal isogeometric method for linear elliptic problems,” *Computational Mechanics*, vol. 68, no. 6, pp. 1385–1405, 2021.
- [38] P. Antolín, X. Wei, and A. Buffa, “Robust numerical integration on curved polyhedra based on folded decompositions,” *Computer Methods in Applied Mechanics and Engineering*, vol. 395, p. 114948, 2022.
- [39] H. C. Kuhlmann and F. Romanò, “The lid-driven cavity,” *Computational Modelling of Bifurcations and Instabilities in Fluid Dynamics*, pp. 233–309, 2019.
- [40] P. Clément, “Approximation by finite element functions using local regularization,” *ESAIM: Mathematical Modelling and Numerical Analysis - Modélisation Mathématique et Analyse Numérique*, vol. 9, no. R2, pp. 77–84, 1975.
- [41] C. Bernardi and V. Girault, “A local regularization operator for triangular and quadrilateral finite elements,” *SIAM Journal on Numerical Analysis*, vol. 35, p. 1893–1916, Oct. 1998.

A Proofs of reliability and efficiency

The proofs of Theorems 2.5 and 2.7 are given in this appendix in the framework of Stokes’ equations. Note that the proofs in the context of linear elasticity and Poisson’s problems are very similar. From the proofs for Stokes’ equations, one only needs to remove the pressure terms and the divergence condition everywhere to obtain the proofs for the linear elasticity problem. One moreover needs to consider the scalar problems equivalent to the vectorial problems to obtain the proofs for Poisson’s equation.

To ease the notation in the following analysis, we respectively denote the Neumann boundaries of Ω_0 and of \tilde{F}_p^k by $\Gamma_N^0 := (\Gamma_N \setminus \gamma) \cup \gamma_0$, $\tilde{\Gamma}_N^k := \gamma_s^k \cup \tilde{\gamma}^k$, for all $k = 1, \dots, N_f$, and we let $\tilde{\Gamma}_N := \bigcup_{k=1}^{N_f} \tilde{\Gamma}_N^k = \gamma_s \cup \tilde{\gamma}$.

A.1 Reliability

In this section, we prove Theorem 2.5 in the context of Stokes’ equations. That is, under Assumptions 2.1 and 2.4, we prove that the error indicator defined in (29) is reliable, i.e., it is an upper bound for the defeating error.

Proof. Let $\mathbf{e}_u := \mathbf{u} - \mathbf{u}_d \in \mathbf{H}_{0,\Gamma_D}^1(\Omega)$ and $e_p := p - p_d \in L^2(\Omega)$. Let us consider the exact problem (18) restricted to $\Omega_\star = \Omega \setminus \overline{F_p}$ with the natural Neumann boundary condition $\boldsymbol{\sigma}(\mathbf{u})\mathbf{n}_0 - p\mathbf{n}_0$ on $\gamma_{0,p}$, and let us consider the simplified problem (21) also restricted to Ω_\star , with the natural Neumann boundary condition $\boldsymbol{\sigma}(\mathbf{u}_d)\mathbf{n} - p_d\mathbf{n}$ on γ_n . Then, combining both differential problems, for all $(\mathbf{v}_0, q_0) \in \mathbf{H}_{0,\Gamma_D}^1(\Omega_\star) \times L^2(\Omega_\star)$,

$$\begin{aligned} \int_{\Omega_\star} \boldsymbol{\sigma}(\mathbf{e}_u) : \boldsymbol{\varepsilon}(\mathbf{v}_0) \, dx - \int_{\Omega_\star} e_p \nabla \cdot \mathbf{v}_0 \, dx &= \int_{\gamma_n} (\mathbf{g} - \boldsymbol{\sigma}(\mathbf{u}_d)\mathbf{n} + p_d\mathbf{n}) \cdot \mathbf{v}_0 \, ds + \int_{\gamma_{0,p}} (\boldsymbol{\sigma}(\mathbf{u})\mathbf{n}_0 - p\mathbf{n}_0 - \mathbf{g}_0) \cdot \mathbf{v}_0 \, ds, \\ &\quad - \int_{\Omega_\star} q_0 \nabla \cdot \mathbf{e}_u \, dx = 0. \end{aligned} \tag{35}$$

In a very similar fashion, we can deduce that for all $k = 1, \dots, N_f$ and all $(\mathbf{v}^k, q^k) \in \mathbf{H}^1(F_p^k) \times L^2(F_p^k)$,

$$\begin{aligned} \int_{F_p^k} \boldsymbol{\sigma}(\mathbf{e}_u) : \boldsymbol{\varepsilon}(\mathbf{v}^k) dx - \int_{F_p^k} e_p \boldsymbol{\nabla} \cdot \mathbf{v}^k dx &= \int_{\gamma_{0,p}^k} [(\boldsymbol{\sigma}(\mathbf{u}) - \boldsymbol{\sigma}(\mathbf{u}_d)) \mathbf{n}^k - (p - p_d) \mathbf{n}^k] \cdot \mathbf{v}^k ds \\ &\quad + \int_{\gamma_r^k} (\mathbf{g} - \boldsymbol{\sigma}(\mathbf{u}_d) \mathbf{n}^k + p_d \mathbf{n}^k) \cdot \mathbf{v}^k ds, \\ &\quad - \int_{F_p^k} q^k \boldsymbol{\nabla} \cdot \mathbf{e}_u dx = 0. \end{aligned} \quad (36)$$

Therefore, let $(\mathbf{v}, q) \in \mathbf{H}_{0,\Gamma_D}^1(\Omega) \times L^2(\Omega)$, since $\mathbf{n} = \mathbf{n}^{k_\gamma}$ on all $\gamma \in \Sigma_r$, then

$$\mathbf{a}(\mathbf{e}_u, \mathbf{v}) + \mathbf{b}(\mathbf{v}, e_p) = \int_{\Omega} \boldsymbol{\sigma}(\mathbf{e}_u) : \boldsymbol{\varepsilon}(\mathbf{v}) dx - \int_{\Omega} e_p \boldsymbol{\nabla} \cdot \mathbf{v} dx = \sum_{\gamma \in \Sigma} \int_{\gamma} \mathbf{d}_{\gamma} \cdot \mathbf{v} ds, \quad (37)$$

$$\mathbf{b}(\mathbf{e}_u, q) = - \int_{\Omega} q \boldsymbol{\nabla} \cdot \mathbf{e}_u dx = 0. \quad (38)$$

The right hand side of (37) can be rewritten

$$\sum_{\gamma \in \Sigma} \int_{\gamma} \mathbf{d}_{\gamma} \cdot \mathbf{v} ds = \sum_{\gamma \in \Sigma} \left[\int_{\gamma} (\mathbf{d}_{\gamma} - \overline{\mathbf{d}}_{\gamma}^{\gamma}) \cdot (\mathbf{v} - \overline{\mathbf{v}}^{\gamma}) ds + \overline{\mathbf{d}}_{\gamma}^{\gamma} \cdot \int_{\gamma} \mathbf{v} ds \right]. \quad (39)$$

For each $\gamma \in \Sigma$, the first terms of (37) can be estimated thanks to the Poincaré inequality and trace inequalities, using the domains Ω^k defined in condition (b) of Assumption 2.1 for $k = 1, \dots, N_f$. That is,

$$\begin{aligned} &\sum_{\gamma \in \Sigma} \int_{\gamma} (\mathbf{d}_{\gamma} - \overline{\mathbf{d}}_{\gamma}^{\gamma}) \cdot (\mathbf{v} - \overline{\mathbf{v}}^{\gamma}) ds \\ &\lesssim \sum_{\gamma \in \Sigma} \|\mathbf{d}_{\gamma} - \overline{\mathbf{d}}_{\gamma}^{\gamma}\|_{0,\gamma} \|\mathbf{v} - \overline{\mathbf{v}}^{\gamma}\|_{0,\gamma} \lesssim \sum_{\gamma \in \Sigma} |\gamma|^{\frac{1}{2(n-1)}} \|\mathbf{d}_{\gamma} - \overline{\mathbf{d}}_{\gamma}^{\gamma}\|_{0,\gamma} |\mathbf{v}|_{\frac{1}{2},\gamma} \\ &\lesssim \sum_{\gamma \in \Sigma_n \cup \Sigma_r} |\gamma|^{\frac{1}{2(n-1)}} \|\mathbf{d}_{\gamma} - \overline{\mathbf{d}}_{\gamma}^{\gamma}\|_{0,\gamma} \|\mathbf{v}\|_{1,\Omega^{k_\gamma}} + \sum_{\gamma \in \Sigma_{0,p}} |\gamma|^{\frac{1}{2(n-1)}} \|\mathbf{d}_{\gamma} - \overline{\mathbf{d}}_{\gamma}^{\gamma}\|_{0,\gamma} \|\mathbf{v}\|_{1,\Omega^{k_\gamma} \cap \Omega_*}. \end{aligned} \quad (40)$$

Then, the last terms of (39) can be estimated thanks to [1, Appendix A.2] and trace inequalities, that is,

$$\begin{aligned} \overline{\mathbf{d}}_{\gamma}^{\gamma} \cdot \int_{\gamma} \mathbf{v} ds &\lesssim |\gamma|^{\frac{1}{2}} \|\overline{\mathbf{d}}_{\gamma}^{\gamma}\|_{\ell^2} \|\mathbf{v}\|_{0,\gamma} \\ &\lesssim \sum_{\gamma \in \Sigma_n \cup \Sigma_r} c_{\gamma} |\gamma|^{\frac{n}{2(n-1)}} \|\overline{\mathbf{d}}_{\gamma}^{\gamma}\|_{\ell^2} \|\mathbf{v}\|_{\frac{1}{2},\partial\Omega^{k_\gamma}} + \sum_{\gamma \in \Sigma_{0,p}} c_{\gamma} |\gamma|^{\frac{n}{2(n-1)}} \|\overline{\mathbf{d}}_{\gamma}^{\gamma}\|_{\ell^2} \|\mathbf{v}\|_{\frac{1}{2},\partial(\Omega^{k_\gamma} \cap \Omega_*)} \\ &\lesssim \sum_{\gamma \in \Sigma_n \cup \Sigma_r} c_{\gamma} |\gamma|^{\frac{n}{2(n-1)}} \|\overline{\mathbf{d}}_{\gamma}^{\gamma}\|_{\ell^2} \|\mathbf{v}\|_{1,\Omega^{k_\gamma}} + \sum_{\gamma \in \Sigma_{0,p}} c_{\gamma} |\gamma|^{\frac{n}{2(n-1)}} \|\overline{\mathbf{d}}_{\gamma}^{\gamma}\|_{\ell^2} \|\mathbf{v}\|_{1,\Omega^{k_\gamma} \cap \Omega_*}. \end{aligned} \quad (41)$$

Thus combining (39), (40) and (41), defining $\hat{\mathcal{E}}(\mathbf{u}_d, p_d) := \mu^{\frac{1}{2}} \mathcal{E}(\mathbf{u}_d, p_d)$, for all $\mathbf{v} \in \mathbf{H}_{0,\Gamma_D}^1(\Omega)$,

$$\sum_{\gamma \in \Sigma} \int_{\gamma} \mathbf{d}_{\gamma} \cdot \mathbf{v} ds \lesssim \hat{\mathcal{E}}(\mathbf{u}_d, p_d) \|\boldsymbol{\nabla} \mathbf{v}\|_{0,\Omega}. \quad (42)$$

Now, remark that if we take $\mathbf{v} = \mathbf{e}_u \in \mathbf{H}_{0,\Gamma_D}^1(\Omega)$ and $q = e_p \in L^2(\Omega)$, then equation (38) reads $\mathbf{b}(\mathbf{e}_u, e_p) = 0$, and thus using (42), equation (37) rewrites

$$\mathbf{a}(\mathbf{e}_u, \mathbf{e}_u) = \int_{\Omega} \boldsymbol{\sigma}(\mathbf{e}_u) : \boldsymbol{\varepsilon}(\mathbf{e}_u) dx - \int_{\Omega} e_p \boldsymbol{\nabla} \cdot \mathbf{e}_u dx = \sum_{\gamma \in \Sigma} \int_{\gamma} \mathbf{d}_{\gamma} \cdot \mathbf{e}_u ds \lesssim \hat{\mathcal{E}}(\mathbf{u}_d, p_d) \|\boldsymbol{\nabla} \mathbf{e}_u\|_{0,\Omega}.$$

Using the coercivity of $\mathbf{a}(\cdot, \cdot)$ in $\mathbf{H}_{0,\Gamma_D}^1(\Omega)$ equipped with the norm $\|\nabla \cdot\|_{0,\Omega}$, then

$$\mathbf{a}(\mathbf{e}_u, \mathbf{e}_u) \lesssim \hat{\mathcal{E}}(\mathbf{u}_d, p_d) \|\nabla \mathbf{e}_u\|_{0,\Omega} \lesssim \mu^{-\frac{1}{2}} \hat{\mathcal{E}}(\mathbf{u}_d, p_d) (\mathbf{a}(\mathbf{e}_u, \mathbf{e}_u))^{\frac{1}{2}} \quad (43)$$

so that if we simplify on both sides,

$$(\mathbf{a}(\mathbf{e}_u, \mathbf{e}_u))^{\frac{1}{2}} \lesssim \mathcal{E}(\mathbf{u}_d, p_d). \quad (44)$$

Finally, since $\mathbf{b}(\cdot, \cdot)$ satisfies the inf-sup condition, using (37) and (42), using the continuity of $\mathbf{a}(\cdot, \cdot)$ in $\mathbf{H}_{0,\Gamma_D}^1(\Omega)$, and then its coercivity as in (43), then

$$\begin{aligned} \|e_p\|_{0,\Omega} &\lesssim \sup_{\substack{\mathbf{v} \in \mathbf{H}_{0,\Gamma_D}^1(\Omega) \\ \mathbf{v} \neq \mathbf{0}}} \frac{\mathbf{b}(\mathbf{v}, e_p)}{\|\nabla \mathbf{v}\|_{0,\Omega}} = \sup_{\substack{\mathbf{v} \in \mathbf{H}_{0,\Gamma_D}^1(\Omega) \\ \mathbf{v} \neq \mathbf{0}}} \frac{\sum_{\gamma \in \Sigma} \int_{\gamma} \mathbf{d}_{\gamma} \cdot \mathbf{v} \, ds - \mathbf{a}(\mathbf{e}_u, \mathbf{v})}{\|\nabla \mathbf{v}\|_{0,\Omega}} \\ &\leq \sup_{\substack{\mathbf{v} \in \mathbf{H}_{0,\Gamma_D}^1(\Omega) \\ \mathbf{v} \neq \mathbf{0}}} \frac{\sum_{\gamma \in \Sigma} \int_{\gamma} \mathbf{d}_{\gamma} \cdot \mathbf{v} \, ds}{\|\nabla \mathbf{v}\|_{0,\Omega}} - \inf_{\substack{\mathbf{v} \in \mathbf{H}_{0,\Gamma_D}^1(\Omega) \\ \mathbf{v} \neq \mathbf{0}}} \frac{\mathbf{a}(\mathbf{e}_u, \mathbf{v})}{\|\nabla \mathbf{v}\|_{0,\Omega}} \\ &\lesssim \hat{\mathcal{E}}(\mathbf{u}_d, p_d) + \|\nabla \mathbf{e}_u\|_{0,\Omega} \lesssim \hat{\mathcal{E}}(\mathbf{u}_d, p_d) + \mu^{\frac{1}{2}} (\mathbf{a}(\mathbf{e}_u, \mathbf{e}_u))^{\frac{1}{2}} \lesssim \hat{\mathcal{E}}(\mathbf{u}_d, p_d). \end{aligned} \quad (45)$$

We can therefore conclude by combining (44) and (45). \square

A.2 Efficiency

In this section, we prove Theorem 2.7 in the context of Stokes' equations. That is, we prove that the error indicator defined in (29) is efficient under Assumptions 2.1 and 2.4, i.e., it is a lower bound for the defeating error, up to oscillations. The proof is given in the general case for $n = 3$, but under the following additional assumption if $n = 2$:

Assumption A.1 If $n = 2$, assume that the compatibility conditions (23) and (26) are satisfied.

Note however that the numerical experiments show that the result also holds without compatibility conditions if $n = 2$. The same restrictions were considered in the efficiency proofs of [1] in the two-dimensional case.

In the following, for all $D \subset \mathbb{R}^n$ and $\Lambda \subset \partial D$, we denote by $H_{00}^{\frac{1}{2}}(\Lambda)$ the space of functions $w \in L^2(\Lambda)$ such that the zero-extension w^* of w to ∂D belongs to $H^{\frac{1}{2}}(\partial D)$, and we denote by $H_{00}^{-\frac{1}{2}}(\Lambda)$ its dual space. For the sake of simplicity, let us strengthen Definition 2.6, even though the proofs could be easily generalized to the weaker setting.

Definition A.2 An $(n-1)$ -dimensional subset Λ of \mathbb{R}^n is *regular* if Λ is piecewise shape regular and composed of flat elements, that is, if there is $N_{\Lambda} \in \mathbb{N}$ such that for all $\ell_1, \ell_2 = 1, \dots, N_{\Lambda}$ with $\ell_1 \neq \ell_2$, $\Lambda = \text{int} \left(\bigcup_{\ell=1}^{N_{\Lambda}} \Lambda^{\ell} \right)$, $\Lambda^{\ell_1} \cap \Lambda^{\ell_2} = \emptyset$, $|\Lambda| \lesssim |\Lambda^{\ell_1}|$ and Λ^{ℓ_1} is flat, i.e. it is a straight line if $n = 2$ or a flat square or triangle if $n = 3$.

That is, we suppose that the boundaries $\gamma \in \Sigma$ of the features are shape regular as in Definition A.2 instead of Definition 2.6, for simplicity. This allows us to easily define the following Cl  ment operator. Whenever some boundary Λ is regular, then for all $m \in \mathbb{N}$, let $\mathbb{Q}_{m,0}^{\text{pw}}(\Lambda)$ be the space of continuous piecewise polynomials of degree at most m on each variable, that vanish at the boundary $\partial \Lambda$. Then we define

$$\Pi_{m,\Lambda} : L^2(\Lambda) \rightarrow \mathbb{Q}_{m,0}^{\text{pw}}(\Lambda) \quad (46)$$

as the extension of the Cl  ment operator [40] developed in [41] on Λ .

In this context, we define the oscillations appearing in the upper bound of Theorem 2.7 as follows:

Definition A.3 For any $m \in \mathbb{N}$, let $\mathbf{\Pi}_m$ be such that $\mathbf{\Pi}_m|_{\gamma} \equiv \mathbf{\Pi}_{m,\gamma}$ for all $\gamma \in \Sigma$, where $\mathbf{\Pi}_{m,\gamma}$ is the component-wise extensions of the Clément operator defined in (46), and let \mathbf{d}^k be such that $\mathbf{d}^k|_{\gamma} \equiv \mathbf{d}_{\gamma}$ on all $\gamma \in \Sigma^k$, for all $k = 1, \dots, N_f$. Then we define

$$\text{osc}(\mathbf{u}_d, p_d)^2 := \sum_{k=1}^{N_f} (\text{osc}^k(\mathbf{u}_d, p_d))^2, \quad \text{with} \quad \text{osc}^k(\mathbf{u}_d, p_d) := |\Gamma^k|^{\frac{1}{2(n-1)}} \left\| \mathbf{d}^k - \mathbf{\Pi}_m(\mathbf{d}^k) \right\|_{0,\Gamma^k} \quad \text{for } k = 1, \dots, N_f.$$

Let us finally give the proof of Theorem 2.7 under Assumption A.1.

Proof. Let $\mathbf{e}_u := \mathbf{u} - \mathbf{u}_d \in \mathbf{H}_{0,\Gamma_D}^1(\Omega)$, let $e_p := p - p_d \in L^2(\Omega)$, let $k \in \{1, \dots, N_f\}$, and let $\Omega_{\star}^k := \Omega_{\star} \cap \Omega^k$, where Ω^k is the domain associated to feature F^k defined in condition (b) of Assumption 2.1. Then, let us consider the exact problem (18) restricted to Ω_{\star}^k with the natural Neumann boundary condition $\boldsymbol{\sigma}(\mathbf{u})\mathbf{n}_0 - p\mathbf{n}_0$ on $\gamma_{0,p}^k$ and the natural Dirichlet boundary condition $\text{tr}_{\partial\Omega_{\star}^k \setminus \partial\Omega_{\star}}(\mathbf{u})$ on $\partial\Omega_{\star}^k \setminus \partial\Omega_{\star}$, and let us consider the simplified problem (21) also restricted to Ω_{\star}^k , with the natural Neumann boundary condition $\boldsymbol{\sigma}(\mathbf{u}_d)\mathbf{n} - p_d\mathbf{n}$ on γ_n^k , and the natural Dirichlet boundary condition $\text{tr}_{\partial\Omega_{\star}^k \setminus \partial\Omega_{\star}}(\mathbf{u}_d)$ on $\partial\Omega_{\star}^k \setminus \partial\Omega_{\star}$. Then, combining both differential problems, for all $(\mathbf{v}_0, q_0) \in \mathbf{H}_{0,\partial\Omega_{\star}^k \setminus [\Gamma_N \cup \gamma_{0,p}^k]}^1(\Omega_{\star}^k) \times L^2(\Omega_{\star}^k)$,

$$\begin{aligned} \int_{\Omega_{\star}^k} \boldsymbol{\sigma}(\mathbf{e}_u) : \boldsymbol{\varepsilon}(\mathbf{v}_0) \, dx - \int_{\Omega_{\star}^k} e_p \nabla \cdot \mathbf{v}_0 \, dx &= \int_{\gamma_n^k} (\mathbf{g} - \boldsymbol{\sigma}(\mathbf{u}_d)\mathbf{n} + p_d\mathbf{n}) \cdot \mathbf{v}_0 \, ds + \int_{\gamma_{0,p}^k} (\boldsymbol{\sigma}(\mathbf{u})\mathbf{n}_0 - p\mathbf{n}_0 - \mathbf{g}_0) \cdot \mathbf{v}_0 \, ds, \\ &\quad - \int_{\Omega_{\star}^k} q_0 \nabla \cdot \mathbf{e}_u \, dx = 0. \end{aligned} \quad (47)$$

Let $(\mathbf{v}, q) \in \mathbf{H}_{0,\partial\Omega^k \setminus \Gamma_N}^1(\Omega^k) \times L^2(\Omega^k)$, and recall that $\Omega_{\star} = \Omega \setminus \overline{F_p}$, so that $\Omega^k = \text{int}(F_p^k \cup \Omega_{\star}^k)$. Consequently, reusing equation (36),

$$\begin{aligned} &\int_{\Omega^k} \boldsymbol{\sigma}(\mathbf{e}_u) : \boldsymbol{\varepsilon}(\mathbf{v}) \, dx - \int_{\Omega^k} e_p \nabla \cdot \mathbf{v} \, dx \\ &= \int_{\gamma_n^k} (\mathbf{g} - \boldsymbol{\sigma}(\mathbf{u}_d)\mathbf{n} + p_d\mathbf{n}) \cdot \mathbf{v} \, ds + \int_{\gamma_{0,p}^k} (-\mathbf{g}_0 - \boldsymbol{\sigma}(\mathbf{u}_d)\mathbf{n}^k + p_d\mathbf{n}^k) \cdot \mathbf{v} \, ds + \int_{\gamma_t^k} (\mathbf{g} - \boldsymbol{\sigma}(\mathbf{u}_d)\mathbf{n}^k + p_d\mathbf{n}^k) \cdot \mathbf{v} \, ds \\ &= \sum_{\gamma \in \Sigma^k} \int_{\gamma} \mathbf{d}_{\gamma} \cdot \mathbf{v} \, ds, \quad \text{and} \quad - \int_{\Omega^k} q \nabla \cdot \mathbf{e}_u \, dx = 0. \end{aligned} \quad (48)$$

Now, let $\mathbf{a}^k(\cdot, \cdot) : \mathbf{H}_{0,\partial\Omega^k \setminus \Gamma_N}^1(\Omega^k) \times \mathbf{H}_{0,\partial\Omega^k \setminus \Gamma_N}^1(\Omega^k) \rightarrow \mathbb{R}$ and $\mathbf{b}^k(\cdot, \cdot) : \mathbf{H}_{0,\partial\Omega^k \setminus \Gamma_N}^1(\Omega^k) \times L^2(\Omega^k) \rightarrow \mathbb{R}$ be defined by

$$\begin{aligned} \mathbf{a}^k(\mathbf{w}, \mathbf{v}) &= \int_{\Omega^k} \boldsymbol{\sigma}(\mathbf{w}) : \boldsymbol{\varepsilon}(\mathbf{v}) \, dx, & \forall \mathbf{w}, \mathbf{v} \in \mathbf{H}_{0,\partial\Omega^k \setminus \Gamma_N}^1(\Omega^k), \\ \mathbf{b}^k(\mathbf{v}, q) &= - \int_{\Omega^k} q \nabla \cdot \mathbf{v} \, dx, & \forall \mathbf{v} \in \mathbf{H}_{0,\partial\Omega^k \setminus \Gamma_N}^1(\Omega^k), \forall q \in L^2(\Omega^k). \end{aligned}$$

Note that $\mathbf{a}^k(\cdot, \cdot)$ and $\mathbf{b}^k(\cdot, \cdot)$ are continuous with respect to the norms $\|\nabla \cdot\|_{0,\Omega^k}$ for $\mathbf{H}_{0,\partial\Omega^k \setminus \Gamma_N}^1(\Omega^k)$, and $\|\cdot\|_{0,\Omega^k}$ for $L^2(\Omega^k)$. Thus using (48), for all $\mathbf{v} \in \mathbf{H}_{0,\partial\Omega^k \setminus \Gamma_N}^1(\Omega^k)$,

$$\sum_{\gamma \in \Sigma^k} \int_{\gamma} \mathbf{d}_{\gamma} \cdot \mathbf{v} \, ds = \mathbf{a}^k(\mathbf{e}_u, \mathbf{v}) + \mathbf{b}^k(\mathbf{v}, e_p) \lesssim \mu (\|\nabla \mathbf{e}_u\|_{0,\Omega^k} + \|e_p\|_{0,\Omega^k}) \|\nabla \mathbf{v}\|_{0,\Omega^k}. \quad (49)$$

Furthermore, let $\mathbf{H}^{(k)} := \left\{ \mathbf{v} \in \mathbf{H}_{00}^{\frac{1}{2}}(\Gamma^k) : \mathbf{v}|_{\gamma} \in \mathbf{H}_{00}^{\frac{1}{2}}(\gamma), \text{ for all } \gamma \in \Sigma^k \right\}$ equipped with the norm

$$\|\cdot\|_{\mathbf{H}^{(k)}} := \left(\sum_{\gamma \in \Sigma^k} \|\cdot\|_{\mathbf{H}_{00}^{1/2}(\gamma)}^2 \right)^{\frac{1}{2}},$$

and let $(\mathbf{H}^{(k)})^*$ be its dual space equipped with the dual norm $\|\cdot\|_{(\mathbf{H}^{(k)})^*}$. For all $\mathbf{w} \in \mathbf{H}^{(k)}$, let us define piecewise $\mathbf{u}_{\mathbf{w}} \in \mathbf{H}_{\mathbf{0}, \partial\Omega^k \setminus (\gamma_n^k \cup \gamma_r^k)}^1(\Omega^k) \subset \mathbf{H}_{\mathbf{0}, \partial\Omega^k \setminus \Gamma_N}^1(\Omega^k)$ as the unique solution of

$$\begin{cases} -\nabla \cdot \boldsymbol{\sigma}(\mathbf{u}_{\mathbf{w}}|_{F_p^k}) = \mathbf{0} & \text{in } F_p^k \\ \mathbf{u}_{\mathbf{w}}|_{F_p^k} = (\mathbf{w}|_{\gamma_{0,p}^k \cup \gamma_r^k})^* & \text{on } \partial F_p^k, \end{cases} \quad \begin{cases} -\nabla \cdot \boldsymbol{\sigma}(\mathbf{u}_{\mathbf{w}}|_{\Omega_\star^k}) = \mathbf{0} & \text{in } \Omega_\star^k \\ \mathbf{u}_{\mathbf{w}}|_{\Omega_\star^k} = (\mathbf{w}|_{\gamma_{0,p}^k \cup \gamma_n^k})^* & \text{on } \partial\Omega_\star^k, \end{cases}$$

where $(\mathbf{w}|_{\gamma_{0,p}^k \cup \gamma_r^k})^*$ and $(\mathbf{w}|_{\gamma_{0,p}^k \cup \gamma_n^k})^*$ are the extensions by $\mathbf{0}$ of $\mathbf{w}|_{\gamma_{0,p}^k \cup \gamma_r^k}$ on ∂F_p^k and of $\mathbf{w}|_{\gamma_{0,p}^k \cup \gamma_n^k}$ on $\partial\Omega_\star^k$, respectively. Then by continuity of the solution on the data and from [1, Appendix A.6],

$$\|\nabla \mathbf{u}_{\mathbf{w}}\|_{0, \Omega^k} \lesssim \left(\|\mathbf{w}\|_{\mathbf{H}_{00}^{1/2}(\gamma_{0,p}^k \cup \gamma_r^k)}^2 + \|\mathbf{w}\|_{\mathbf{H}_{00}^{1/2}(\gamma_{0,p}^k \cup \gamma_n^k)}^2 \right)^{\frac{1}{2}} \lesssim \|\mathbf{w}\|_{\mathbf{H}^{(k)}}. \quad (50)$$

So thanks to (49) and (50), recalling that $\mathbf{d}^k|_{\gamma} = \mathbf{d}_{\gamma}$ on each $\gamma \in \Sigma^k$ by definition, then

$$\begin{aligned} \|\mathbf{d}^k\|_{(\mathbf{H}^{(k)})^*} &= \sup_{\substack{\mathbf{w} \in \mathbf{H}^{(k)} \\ \mathbf{w} \neq \mathbf{0}}} \frac{\int_{\Gamma^k} \mathbf{d}^k \cdot \mathbf{w} \, ds}{\|\mathbf{w}\|_{\mathbf{H}^{(k)}}} \lesssim \sup_{\substack{\mathbf{w} \in \mathbf{H}^{(k)} \\ \mathbf{w} \neq \mathbf{0}}} \frac{\sum_{\gamma \in \Sigma^k} \int_{\gamma} \mathbf{d}_{\gamma} \cdot \mathbf{u}_{\mathbf{w}} \, ds}{\|\nabla \mathbf{u}_{\mathbf{w}}\|_{0, \Omega^k}} \\ &\leq \sup_{\substack{\mathbf{v} \in \mathbf{H}_{\mathbf{0}, \partial\Omega^k \setminus \Gamma_N}^1(\Omega^k) \\ \mathbf{v} \neq \mathbf{0}}} \frac{\sum_{\gamma \in \Sigma^k} \int_{\gamma} \mathbf{d}_{\gamma} \cdot \mathbf{v} \, ds}{\|\nabla \mathbf{v}\|_{0, \Omega^k}} \lesssim \mu \|\nabla \mathbf{e}\|_{0, \Omega^k}. \end{aligned} \quad (51)$$

Moreover, using Remark 4.6 if $n = 3$, or Remark 4.5 if $n = 2$ and the data compatibility conditions (23) and (26) are satisfied, then

$$\mathcal{E}(\mathbf{u}_d) \lesssim \mu^{-\frac{1}{2}} \left(\sum_{k=1}^{N_f} \sum_{\gamma \in \Sigma^k} |\gamma|^{\frac{1}{n-1}} \|\mathbf{d}_{\gamma}\|_{0, \gamma}^2 \right)^{\frac{1}{2}}.$$

Therefore, using the triangle inequality and since $|\gamma_n^k| \simeq |\gamma_r^k| \simeq |\gamma_{0,p}^k| \simeq |\Gamma^k|$ for all $k = 1, \dots, N_f$, then

$$\begin{aligned} \sum_{\gamma \in \Sigma^k} |\gamma|^{\frac{1}{n-1}} \|\mathbf{d}_{\gamma}\|_{0, \gamma}^2 &\lesssim \sum_{\gamma \in \Sigma^k} |\gamma|^{\frac{1}{n-1}} \left(\|\Pi_m(\mathbf{d}_{\gamma})\|_{0, \gamma}^2 + \|\mathbf{d}_{\gamma} - \Pi_m(\mathbf{d}_{\gamma})\|_{0, \gamma}^2 \right) \\ &\lesssim |\Gamma^k|^{\frac{1}{n-1}} \left\| \Pi_m(\mathbf{d}^k) \right\|_{0, \Gamma^k}^2 + |\Gamma^k|^{\frac{1}{n-1}} \left\| \mathbf{d}^k - \Pi_m(\mathbf{d}^k) \right\|_{0, \Gamma^k}^2. \end{aligned}$$

Now, we use the definition of the broken norm in $\mathbf{H}^{(k)}$ to apply the inverse inequality of [1, Appendix A.7]. Recalling Definition A.3 and using again the triangle inequality, we thus obtain for all $k = 1, \dots, N_f$,

$$\begin{aligned} \sum_{\gamma \in \Sigma^k} |\gamma|^{\frac{1}{n-1}} \|\mathbf{d}_{\gamma}\|_{0, \gamma}^2 &\lesssim \left\| \Pi_m(\mathbf{d}^k) \right\|_{(\mathbf{H}^{(k)})^*}^2 + \mu (\text{osc}^k(\mathbf{u}_d))^2 \\ &\lesssim \left\| \mathbf{d}^k \right\|_{(\mathbf{H}^{(k)})^*}^2 + \left\| \Pi_m(\mathbf{d}^k) - \mathbf{d}^k \right\|_{(\mathbf{H}^{(k)})^*}^2 + \mu (\text{osc}^k(\mathbf{u}_d))^2. \end{aligned}$$

Finally, using (51), applying [1, Appendix A.4 and A.6], we obtain

$$\begin{aligned}
\mathcal{E}(\mathbf{u}_d)^2 &\lesssim \mu^{-1} \left(\sum_{k=1}^{N_f} \|\mathbf{d}^k\|_{(\mathbf{H}^{(k)})^*}^2 + \sum_{k=1}^{N_f} \left\| \mathbf{\Pi}_m(\mathbf{d}^k) - \mathbf{d}^k \right\|_{(\mathbf{H}^{(k)})^*}^2 + \mu \operatorname{osc}(\mathbf{u}_d)^2 \right) \\
&\lesssim \mu^{-1} \left(\mu^2 \sum_{k=1}^{N_f} \|\nabla \mathbf{e}\|_{0,\Omega^k}^2 + \sum_{k=1}^{N_f} \left\| \mathbf{\Pi}_m(\mathbf{d}^k) - \mathbf{d}^k \right\|_{\mathbf{H}_{00}^{-1/2}(\Gamma^k)}^2 + \mu \operatorname{osc}(\mathbf{u}_d)^2 \right) \\
&\lesssim \mu \|\nabla \mathbf{e}\|_{0,\Omega}^2 + \operatorname{osc}(\mathbf{u}_d)^2 \lesssim \left(\mu^{\frac{1}{2}} \|\nabla \mathbf{e}\|_{0,\Omega} + \operatorname{osc}(\mathbf{u}_d) \right)^2.
\end{aligned}$$

To conclude, we use the coercivity of the bilinear form $\mathfrak{a}(\cdot, \cdot)$ in $\mathbf{H}_{\mathbf{0},\Gamma_D}^1(\Omega)$ to obtain $\mu^{\frac{1}{2}} \|\nabla \mathbf{e}\|_{0,\Omega} \lesssim \|\mathbf{e}\|_{\Omega}$. \square